The Ising model for the bcc, fcc and diamond lattices; a comparison

P. H. Lundow,[1,*] K. Markström,[2,†] and A. Rosengren[1,‡]

[1] *Condensed Matter Theory, Department of Theoretical Physics, KTH, SE-106 91 Stockholm, Sweden*

[2] *Department of Mathematics, Umeå University, SE-901 87 Umeå, Sweden*

Abstract

A large scale Monte Carlo simulation study of the Ising model for the simple cubic lattice was recently performed by us. In this article we complement that study with the bcc, fcc and diamond lattices. Both the canonical and microcanonical ensembles are employed. We give estimates of the critical temperature and also other quantities in the critical region. An analysis of the critical behaviour points to distinct high- and low-temperature exponents, especially for the specific heat, as was obtained also for the simple cubic lattice, although the agreement is good between the different lattices. The source of this discrepancy is briefly discussed.

*Email: phl@kth.se

†Email: klas.markstrom@math.umu.se

‡Email: roseng@kth.se

Contents

I. Introduction 2

II. Notation and basic definitions 4

III. Physical quantities 6

A. Plots 6

B. Critical points 9

1. The bcc lattice 9

2. The fcc lattice 12

3. The diamond lattice 14

C. Critical values 16

D. Critical exponents 22

IV. Combinatorial quantities 31

A. Plots 31

B. Critical points and values 33

C. Critical exponents 39

V. Discussion 42

Acknowledgements 45

References 45

I. INTRODUCTION

The Ising model was formulated as a model for a uniaxial magnetic system and has become one of the most studied models in theoretical physics. It was solved by Ernst Ising in 1925 [1] in the one-dimensional case, though the solution contained no finite-temperature phase transition. It took almost twenty years before Lars Onsager published the solution for the (infinite) two-dimensional case without an applied field [2]. Being one of the very few exactly solved models, it now serves as a proving ground for new theories, approximations,

and numerical algorithms. Despite many attempts the three-dimensional model has not been solved.

Since the 1960s it has become standard to assume that the scaling hypothesis holds for the free energy of several statistical physics models, among them the Ising model. This is not an unreasonable assumption since it actually is true for the very few cases where there are exact solutions, such as the two-dimensional Ising model. The hypothesis leads to the rather attractive consequence that the high- and low-temperature critical exponents are equal, ie $\alpha = \alpha'$ and $\gamma = \gamma'$. With the advent of renormalization theory the scaling hypothesis received an underlying mechanism, see [3, 4].

The Ising model has been studied using several theoretical approaches, such as high- and low-temperature series expansions, Monte Carlo simulations, both infinite volume and renormalization group methods, and perturbative field theoretical methods, see eg [5–11]. A more extensive list of methods and references can be found in the exhaustive review article by Pelissetto and Vicari [12]. The results of our calculations are compared throughout the text to recent results obtained by some of these methods.

It is perhaps less well known that the model describes several physical systems, which belong to the Ising universality class, besides uniaxial magnetic systems. These include liquid-vapor transitions in simple fluids, binary mixtures of fluids, ionic fluids, and micellar systems. Also in high-energy physics the three-dimensional Ising model is expected to be of relevance. For more on these applications, again see [12].

In a recent review [13] the Ising model on the simple cubic lattice was studied by means of Monte Carlo simulations data of unprecedented size. In this article we complement this by a study of other three-dimensional lattices, namely the body-centred cubic lattice, the face-centred cubic lattice and the diamond lattice. We have used a sampling scheme presented in detail elsewhere [14] combined with the energy distribution reconstruction technique in [15]. We have estimated a great number of properties of the model in the critical region. The critical temperatures found in this study agree with earlier studies, possibly with the exception of the diamond lattice, references are given in the text.

Both the canonical ensemble and the microanonical ensemble were used in the present study. The microcanonical ensemble gives a considerably more detailed picture of the underlying properties for the different lattices, but requires also high-resolution data. For the diamond lattice it revealed a small but distinct extremum in the second derivative of

the entropy clearly outside of the critical region. This corresponds exactly to a very small minimum in the specific heat in the high-temperature region which we would have missed had it not been for the microcanonical ensemble data. We are not aware of any physical significance of this minimum.

By means of conventional analysis using log-log plots we find, in agreement with the study for the simple cubic lattice [13], that the best fit to our data is a collection of distinct high- and low-temperature exponents. A possible "cure" for this, as discussed in [13], is to describe the singularities in terms of a Puiseux-series. There we found that a consequence of this is that correction terms would hide the true asymptotically correct behaviour for lattice sizes obtainable in a foreseeable future. This would in turn have serious implications for the assumptions underlying everyday simulations of lattice systems in statistical mechanics. No attempt to describe the singularities in terms of a Puiseux-series is performed in this paper. The exponents obtained here agree although between the different lattices. The general conclusions regarding finite-size behaviour made in [13] agree with the findings in this paper as well. The reader which is only interested in the results may skip to Tables XIX and XX in Section V.

II. NOTATION AND BASIC DEFINITIONS

The three types of lattices we have studied are the body-centred cubic (bcc), the face-centred cubic (fcc) and the diamond (d) lattice. The bcc lattice is regular of degree 8 and for linear order L it has $L^3/4$ vertices and L^3 edges. The fcc lattice is 12-regular and has $L^3/2$ vertices and $3\,L^3$ edges. The diamond lattice is 4-regular and has $2\,L^3$ vertices and $4\,L^3$ edges. We have used periodic boundary conditions for the bcc and fcc lattice while we imposed helical boundary conditions on the diamond lattice, see chapter 13.1.3 of [16] for details. The bcc and the diamond lattices are both bipartite whereas the fcc is not. Often we will have reason to compare our findings to those in [13], a study of the simple cubic (sc) lattice with periodic boundary conditions. Recall that this lattice is 6-regular with L^3 vertices and $3\,L^3$ edges. We will denote the number of vertices by n and the number of edges by m. Consequently the degree of the lattice is $2\,m/n$.

The energy E of a state $\sigma = (\sigma_1, \sigma_2, \ldots, \sigma_n)$, with $\sigma_i = \pm 1$, is then defined as $E(\sigma) = \sum_{\{i,j\}} \sigma_i\,\sigma_j$, with the sum taken over all the edges $\{i, j\}$, and the magnetisation M is defined

as $M(\sigma) = \sum_i \sigma_i$ with the sum take over all the vertices. Often it is practical to use their normalised forms $U = E/m$ and $\mu = M/n$, so that $-1 \leq U, \mu \leq 1$. The number of states σ having energy E is denoted $a(E)$ while the number of states having energy E and magnetisation M is denoted $a(E, M)$.

There will be two classes of quantities; the combinatorial quantities from the microcanonical esemble which depend on the energy U, and the physical quantities from the canonical ensemble that depend on the coupling, or inverse temperature.

Regarding the definitions of the quantities and exponents we will be consistent with those in [13].

We will briefly state the definitions of the relevant quantities but the details are found in [13]. First the combinatorial quantities beginning with the entropy S, defined at $U = E/m$ as $S(U) = \log[a(E)]/n$ and the coupling defined as $K(U) = -(n/m)\partial S(U)/\partial U$. How to obtain the coupling by sampling is described in detail in [14]. It is occasionally useful to write $\epsilon = (U - U_c)/U_c$.

The average magnetisation is $\mu(U) = \langle M \rangle / n$ and the variance $\chi(U) = \mathrm{Var}(M)/n$, while correspondingly for the absolute magnetisation, $\bar{\mu}(U) = \langle |M| \rangle / n$ and $\bar{\chi}(U) = \mathrm{Var}(|M|)/n$. We look at higher moments as well, denoting

$$\phi(U) = \frac{1}{n} \left\langle (|M| - \langle |M| \rangle)^3 \right\rangle$$
$$\psi(U) = \frac{1}{L^3} \left(\left\langle (|M| - \langle |M| \rangle)^4 \right\rangle - 3 \left\langle (|M| - \langle |M| \rangle)^2 \right\rangle^2 \right)$$

For the physical quantities we start with the partition function

$$\mathcal{Z}(K, H) = \sum_\sigma \exp\left(K\, E(\sigma) + H\, M(\sigma)\right)$$

for a coupling, or inverse temperature, $K = J/k_B T$ and external field H. Replacing the magnetisations with their absolute values gives

$$\overline{\mathcal{Z}}(K, H) = \sum_\sigma \exp\left(K\, E(\sigma) + H\, |M(\sigma)|\right)$$

Of course, no one will be deceived when we write $\mathcal{Z}(K)$ instead of $\mathcal{Z}(K, 0)$, though we could also write

$$\mathcal{Z}(K) = \sum_E a(E)\, \exp(K\, E).$$

Defining the standard quantities is now easy. The free energy is then $\mathcal{F}(K) = (1/n)\log\mathcal{Z}(K)$, the internal energy $\mathcal{U}(K) = (n/m)\,\partial\mathcal{F}(K)/\partial K = \langle E\rangle/m$, the specific heat $\mathcal{C}(K) = \partial\mathcal{U}(K)/\partial K = \mathrm{Var}(E)/m$ and the entropy $\mathcal{S}(K) = \mathcal{F}(K) - (m/n)\,K\,\mathcal{U}(K)$. Note that our definitions of internal energy and specific heat differ by a factor n/m from those usually found in the literature. The coupling (and external field) dependent versions of the magnetisation, susceptibility and higher moments are defined as above, though at a fixed coupling, instead as energy. Equivalently, we let $\bar{\mu}(K)$, $\bar{\chi}(K)$, $\phi(K)$ and $\psi(K)$ denote respectively the first, second, third and fourth derivative of $(1/n)\log\overline{\mathcal{Z}}(K,H)$ with respect to H evaluated at $H = 0$.

Occasionally we may need to subscript the various quantities with the linear size, as in $\mathcal{C}_{16}$ to denote the specific heat for linear size 16. Using these definitions we expect that in the thermodynamical limit, as $L \to \infty$, we will have for example $\mathcal{U}(K(U)) \to U$, $\mathcal{S}(K(U)) \to S(U)$ and $\bar{\mu}(K(U)) \to \bar{\mu}(U)$. That is, the function $K(U)$ translates between the microcanonical and the canonical ensemble, the reader should consult [15] or [14] for more on this. Sometimes we may use the notation $t = (K - K_c)/K_c$.

The study was conducted by Monte Carlo sampling on many different lattice sizes, not entirely consistently chosen, and occasionally on exact data. For the bcc we have used data collected on lattices of linear order $L = 4$, 6, 8, 12, 16, 24, 32, 48, 64, 96, 128, 192 and 256, where the data for $L = 4, 6$ are based upon exact calculations. For fcc we used linear orders $L = 4$, 6, 8, 12, 16, 24, 32, 64, 128 and 256, where $L = 4$ was done exactly. For the diamond lattice we have $L = 4$, 6, 8, 12, 16, 24, 32, 48, 64, 96 and 128 and no exact data. The sc study [13] was done for $L = 4$, 6, 8, 12, 16, 32, 64, 128, 256 and 512 where the data for $L = 4$ are exact.

III. PHYSICAL QUANTITIES

A. Plots

Let us begin by showing some plots of a few physical quantities near the critical coupling. In Figure 1 we show the specific heat $\mathcal{C}(K)$ for the bcc and fcc lattice while Figure 2 shows it for the sc and d lattice. Next the magnetisation $\bar{\mu}(K)$ is shown in Figures 3 and 4. The logarithm of the susceptibility $\bar{\chi}(K)$ is shown in Figures 5 and 6. These plots seem to suggest

a rather similar behaviour near K_c and we are soon going to see just how similar when we estimate the critical exponents.

However, the diamond lattice shows a curious local minimum in the specific heat in the high-temperature region. This minimum corresponds to a maximum in the function $\partial K/\partial U$ which we will study closer in Section IV A. For now we will just state that from a series expansion we receive the location $K \approx 0.128078$ and the value 0.991791.

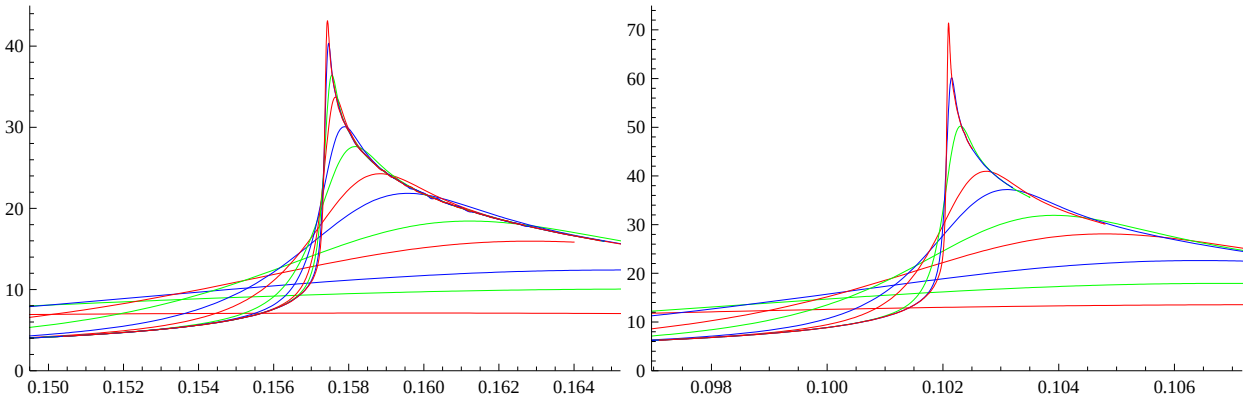

FIG. 1: Specific heat $\mathcal{C}$ vs coupling K for the bcc (left) and fcc (right) lattice near K_c, $-0.05 \leq t \leq 0.05$. Lattice sizes are respectively $L = 4, 6, 8, 12, 16, 24, 32, 48, 64, 96, 128, 192, 256$ and $L = 4, 6, 8, 12, 16, 24, 32, 64, 128, 256$.

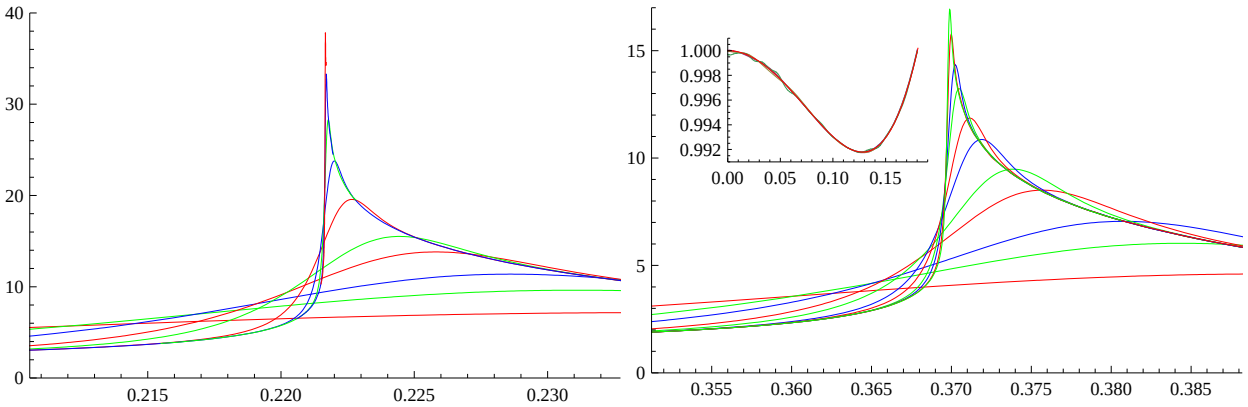

FIG. 2: Specific heat $\mathcal{C}$ vs coupling K for the sc (left) and d (right) lattice near K_c, $-0.05 \leq t \leq 0.05$. Lattice sizes are respectively $L = 4, 6, 8, 12, 16, 32, 64, 128, 256, 512$ and $L = 4, 6, 8, 12, 16, 24, 32, 48, 64, 96, 128$. Inset shows $L = 8, 12, 16, 24$ and a curve (red) obtained from high-temperature series expansion.

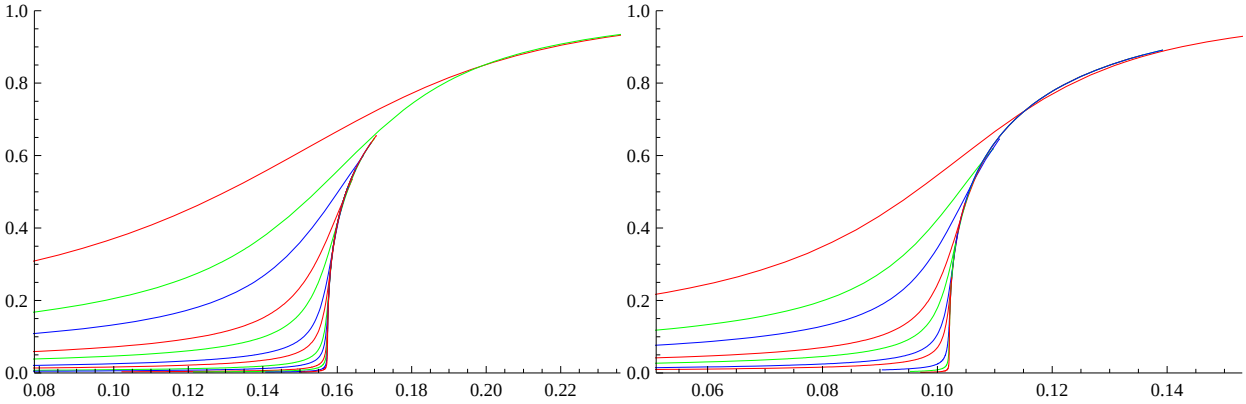

FIG. 3: Magnetisation $\bar{\mu}$ vs coupling K for the bcc (left) and fcc (right) lattice near K_c, $-0.5 \leq t \leq 0.5$. Same lattice sizes as in Figure 1.

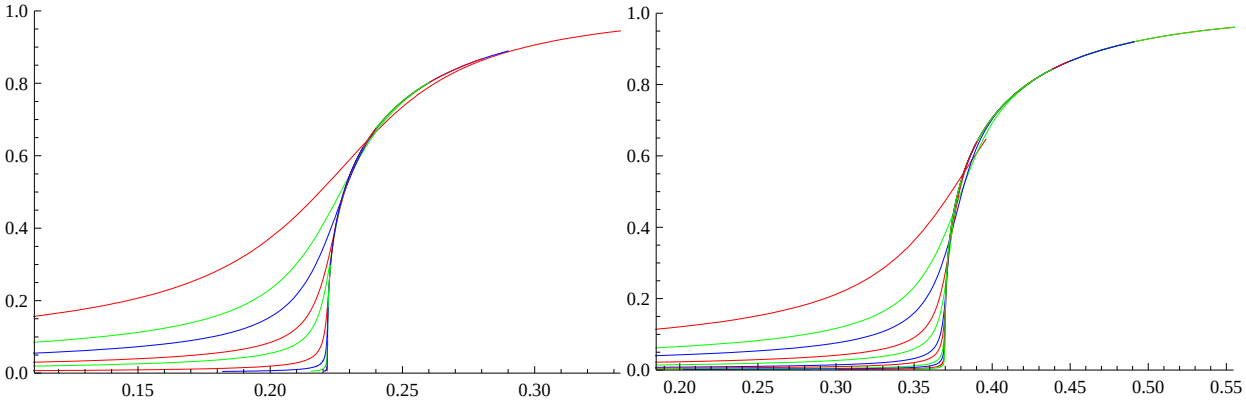

FIG. 4: Magnetisation $\bar{\mu}$ vs coupling K for the sc (left) and d (right) lattice near K_c, $-0.5 \leq t \leq 0.5$. Same lattice sizes as in Figure 2.

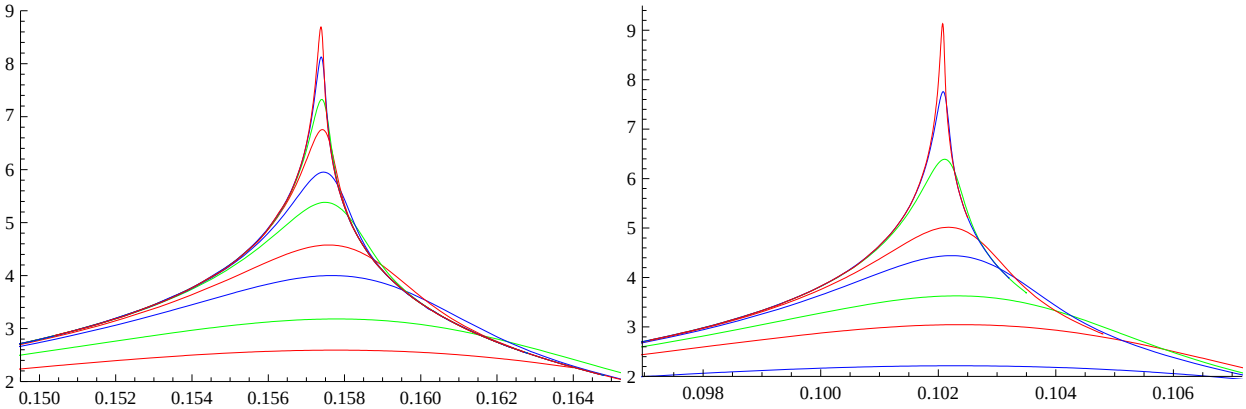

FIG. 5: Logarithmic susceptibility $\log \bar{\chi}$ vs coupling K for the bcc (left) and fcc (right) lattice near K_c, $-0.05 \leq t \leq 0.05$. Lattice sizes are respectively $L = 12, 16, 24, 32, 48, 64, 96, 128, 192, 256$ and $L = 8, 12, 16, 24, 32, 64, 128, 256$.

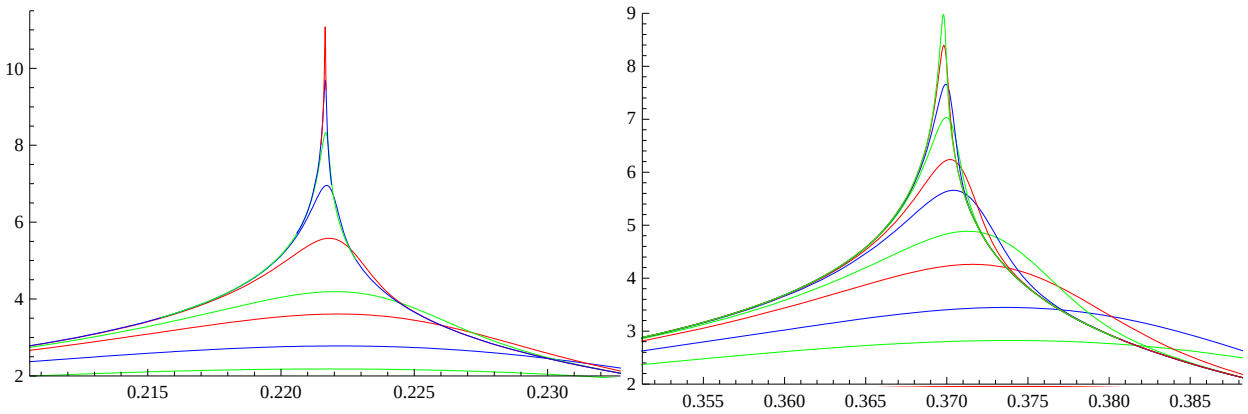

FIG. 6: Logarithmic susceptibility $\log \bar{\chi}$ vs coupling K for the sc (left) and d (right) lattice near K_c, $-0.05 \leq t \leq 0.05$. Lattice sizes are respectively $L = 6, 8, 12, 16, 32, 64, 128, 256, 512$ and $L = 6, 8, 12, 16, 24, 32, 48, 64, 96, 128$.

B. Critical points

First we are going to locate a number of critical points with respect to some quantity and also the values at these points. Since the critical points are assumed to converge towards an asymptotic critical point we will of course estimate that point. The growth rate of the values are also estimated.

The critical points are denoted $K_1^*, \ldots, K_{15}^*$ and are the locations of, respectively, the maximum specific heat $\mathcal{C}$, the maximum and minimum of $\partial\mathcal{C}/\partial K$, the maximum and minimum of $\partial^2\mathcal{C}/\partial K^2$, the maximum of $\partial\bar{\mu}/\partial K$, $\partial \log \bar{\mu}/\partial K$, $\partial \log \chi/\partial K$ and $\bar{\chi}$, the maximum and minimum of ϕ, the minimum and maximum of ψ, the maximum of $\partial\mathcal{Q}/\partial K$ and the crossing point $\mathcal{Q}_L = \mathcal{Q}_{L/2}$. Here $\mathcal{Q}_L$ is the Binder cumulant $\mathcal{Q} = 1 - \langle M^4 \rangle / 3\langle M^2 \rangle^2$ for linear size L.

1. *The bcc lattice*

Beginning with the bcc lattice we list in Table I the critical points $K_1^*, \ldots, K_5^*$, related to the second, third and fourth cumulants with respect to the energy. The points for $L = 8, 12$ in the fourth column are missing since they lie at a too extreme temperature where our method of reconstructing the energy distribution breaks down. Recall that we could easily obtain them for $L = 4, 6$ since they are based upon exact data. We list the points $K_6^*, \ldots, K_{10}^*$ in Table II and $K_{11}^*, \ldots, K_{15}^*$ in Table III. Some points are missing though since they are

outside the range of the collected data.

The asymptotic values in the tables were obtained by fitting points to the formula $c_0 + c_1\, L^{-\lambda}$, where c_0 then would be close to K_c. For the bcc lattice data we fitted the five, six and seven largest cubes ($L \geq 32$, $L \geq 48$, $L \geq 64$, respectively) to this formula. This gave very convincing fitted curves in all cases except for K_2^* and K_{15}^* which show some irregular behaviour. For K_{15}^* (only!) we used instead $L \geq 24$, $L \geq 32$, $L \geq 48$. Thus each sequence of K^* provides us with three measurements, or samplings, of K_c and the medians of these are listed as the asymptotic value. The half-differences between the maxima and the minima can be used as error estimates and are also listed on the last line of the Tables. For K_1^*, for example, the table should then be read as $K_c = 0.157368(2) = 0.157368 \pm 0.000002$. We will work a little more on this in a moment. In Figure 7 these points and the fitted curves are shown.

We could of course have added a correction term and fitted a formula of the form $c_0 + c_1\, L^{-\lambda_1} + c_2\, L^{-\lambda_2}$ to a larger selection of points. This often works very well but the formula can also be rather sensitive as to which points are included in the fit. Note also that when it does work well the resulting c_0 is extremely close to that obtained with the simpler formula for a smaller data set. The benefits of the extra correction term does not seem to add any precision to our estimates of K_c. Thus it seemed wiser to keep it simple.

Looking at the 15 sequences of data we note that some of them are increasing toward some asymptotic value of K_c while others are decreasing. However, some sequences, such as K_9^*, begins by increasing for $L \leq 16$, before turning into a decreasing one. Nevertheless, they all show their true colours for big enough L. We can use these sequences to obtain upper and lower bounds of K_c. Thus, we take the value at $L = 256$ for the decreasing sequences as an upper bound, and the value at $L = 256$ for the increasing sequences as a lower bound. Due to some irregularities in the data we have reason to be slightly suspicious of K_2^* and K_{15}^* so we will exclude them from this affair. The sequences for K_7^* and K_9^* gives us the lower and upper bound respectively

$$0.157370 \leq K_c \leq 0.157382$$

The lower bound is very close to the asymptotic estimates but the upper bound is not very impressive. To improve on this interval we use the asymptotic values as estimates of K_c. After removing the blemished 2nd and 15th sequence, the data set then consists of 13

L	K_1^*	K_2^*	K_3^*	K_4^*	K_5^*
4	0.159462	0.121942	0.197489	0.094288	0.159440
6	0.166310	0.146143	0.185724	0.131927	0.165111
8	0.165277	0.152340		0.143435	0.164056
12	0.162836	0.155756		0.151106	0.161624
16	0.161213	0.156632	0.164752	0.153697	0.160267
24	0.159583	0.157114	0.161332	0.155577	0.158981
32	0.158834	0.157249	0.159908	0.156277	0.158421
48	0.158169	0.157322	0.158715	0.156811	0.157932
64	0.157886	0.157346	0.158228	0.157022	0.157729
96	0.157648	0.157366	0.157819	0.157196	0.157566
128	0.157551	0.157371	0.157663	0.157263	0.157499
192	0.157464	0.157372	0.157520	0.157315	0.157437
256	0.157433	0.157372	0.157470	0.157335	0.157416
∞	0.157368	0.157374	0.157372	0.157370	0.157374
σ	(2)	(2)	(3)	(4)	(4)

TABLE I: Critical points for bcc; location of, respectively, maximum $\mathcal{C}$, maximum and minimum $\partial\mathcal{C}/\partial K$, maximum and minimum $\partial^2\mathcal{C}/\partial K^2$.

points with the minimum 0.157368 and maximum 0.157374. Unfortunately, the minimum falls outside the previously stated interval. However, the median (and mean) of the data set is 0.157371 and taking the 25% and 75% quartile of the data set as lower and upper bounds of K_c we get $K_c = 0.157371(1)$ which will be our final estimate of K_c. In short, after excluding the bad, or at least suspicious, sequences, we take the median of the medians of the asymptotic estimates. Our estimated K_c compares well with other recent estimates, such as [11] who gave $K_c = 0.1573725(6)$, and [17] who gave $K_c = 0.157374(3)$, both of which intersect our estimate.

We move on to the other critical constants $\mathcal{U}_c$, $\mathcal{F}_c$ and $\mathcal{S}_c$. In [13] it proved beneficial to determine these constants by fitting a scaling formula such as above to $\mathcal{U}_L(K_c)$. Choosing different values of K from the interval for K_c above, fitting only on the six largest lattices

L	K_6^*	K_7^*	K_8^*	K_9^*	K_{10}^*
4	0.151789	0.128293	0.121496	0.141834	0.0890632
6	0.160875	0.148075	0.145073	0.154490	0.125303
8	0.161326	0.153108	0.151422	0.156919	0.138106
12	0.160299	0.155899	0.155123	0.157770	0.147784
16	0.159454	0.156649	0.156189	0.157796	0.151450
24	0.158571	0.157088	0.156861	0.157673	0.154333
32	0.158164	0.157222	0.157082	0.157587	0.155469
48	0.157801	0.157304	0.157233	0.157494	0.156378
64	0.157648	0.157334	0.157289	0.157453	0.156748
96	0.157523	0.157358	0.157335	0.157420	0.157049
128	0.157470	0.157364	0.157350	0.157404	0.157167
192	0.157423	0.157369	0.157360	0.157390	0.157268
256	0.157406	0.157370	0.157364	0.157382	0.157305
∞	0.157371	0.157372	0.157371	0.157368	0.157372
σ	(2)	(2)	(2)	(4)	(2)

TABLE II: Critical points for bcc; location of the maximum of, respectively, $\partial\bar{\mu}/\partial K$, $\partial \log \bar{\mu}/\partial K$, $\partial \log \chi/\partial K$, $\bar{\chi}$ and ϕ.

($L \geq 48$), we note that the critical energy is $\mathcal{U}_c = 0.27261(4)$. The same approach for the free energy brings us $\mathcal{F}_c = 0.754006(1)$ and the critical entropy is then $\mathcal{S}_c = \mathcal{F}_c - 4\,K_c\,\mathcal{U}_c = 0.58240(3)$. Unfortunately, only the somewhat dated [18] (see detailed references therein) seem to collect these figures, and from it we extract $\mathcal{U}_c = 0.2732(2)$ and $\mathcal{S} = 0.58203(10)$. Considering how dated these figures are they compare fairly well to our data.

2. The fcc lattice

We will now simply repeat the above for the fcc lattice. The Tables IV, V and VI show the critical points with respect to each quantity for each linear order for the fcc lattice. Again we use different data sets to obtain an estimate of K_c with respect to each quantity. We have used the four, five and six largest lattices when determining the asymptotic values.

L	K^*_{11}	K^*_{12}	K^*_{13}	K^*_{14}	K^*_{15}
4	0.175840	0.136235	0.196968	0.121253	
6	0.170924	0.150271	0.181043	0.143192	
8	0.166860	0.153896		0.149718	0.162289
12	0.162737	0.156019		0.153959	0.158721
16	0.160872	0.156646	0.162773	0.155380	0.157945
24	0.159256	0.157051	0.160236	0.156405	0.157542
32	0.158581	0.157188	0.159196	0.156782	0.157450
48	0.158012	0.157281	0.158334	0.157072	0.157393
64	0.157780	0.157318	0.157982	0.157187	0.157381
96	0.157590	0.157349	0.157696	0.157282	0.157381
128	0.157512	0.157358	0.157580	0.157313	0.157378
192	0.157447	0.157366	0.157480	0.157343	0.157374
256	0.157420	0.157367	0.157441	0.157352	0.157373
∞	0.157374	0.157372	0.157371	0.157369	0.157374
σ	(2)	(2)	(3)	(3)	(2)

TABLE III: Critical points for bcc; location of, respectively, the minimum ϕ, the minimum and maximum ψ, the maximum $\partial\mathcal{Q}/\partial K$ and the crossing point where $\mathcal{Q}_L = \mathcal{Q}_{L/2}$.

This deviates a little from the bcc case of course. Note however, that the seven largest lattices would span linear orders from 12 to 256 and this probably strains our simple scaling formula somewhat. Figure 8 shows these points versus $1/L$ together with the fitted curves.

The curves fit very well to their designated data sets with the exception of K^*_{15} which shows a slightly irregular behaviour. We will therefore exclude it from the rest of this discussion. We note that the sequence that provides us with the best lower bound is K^*_2 and the best upper bound is given by K^*_8; these say

$$0.102070 \leq K_c \leq 0.102075$$

The lower bound is a little suspicious, and indeed the last point for K^*_2 seems to lie ever so slightly above the fitted curves. The error is probably just one step in the last digit though. We continue, as we did for the bcc case and take the median of the medians, using the

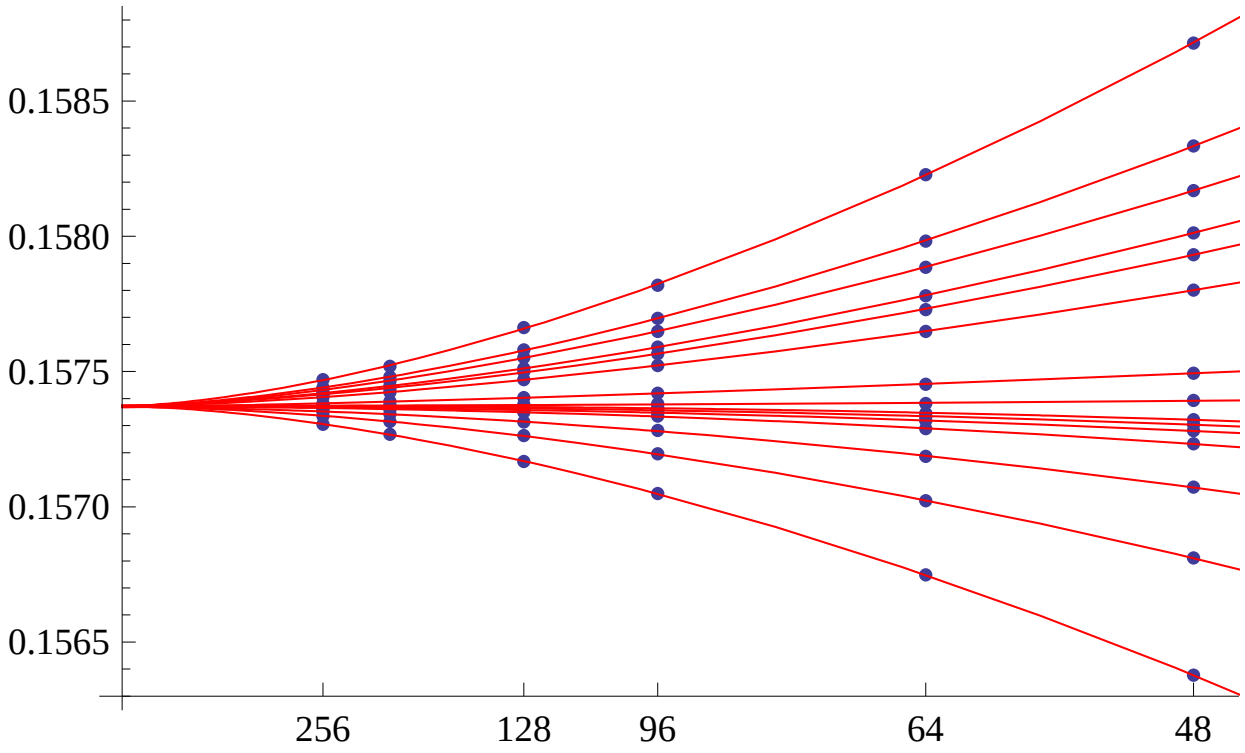

FIG. 7: The critical points $K_1^*, \ldots, K_{15}^*$ vs $1/L$ with fitted curves for the bcc lattice.

first and third quartiles to provide us with error estimates. This gives $K_c = 0.102069(1)$. Again this compares very well with recent estimates. In [17] we find the estimate $K_c = 0.1020705(15)$ which we intersect.

We use the values from our estimated K_c-interval to get sequences of the type $\mathcal{U}_L(K_c)$. Fitting on the five largest lattices gives asymptotic values in the interval $\mathcal{U}_c = 0.24676(6)$. Analogously for the free energy $\mathcal{F}_c = 0.741740(2)$ and thus the critical entropy is $\mathcal{S}_c = \mathcal{F}_c - 6\,K_c\mathcal{U}_c = 0.59062(4)$. Again, from [18] we get $\mathcal{U}_c = 0.24742(5)$ and $\mathcal{S}_c = 0.59023(3)$. These figures match our data acceptably well.

3. The diamond lattice

We move on to the diamond lattice. The critical points are listed in Tables VII, VIII and IX. The quality of these sequences vary and we can probably not aspire to the relatively high precision found in the case of bcc and fcc. Let us first simply note that sequences K_7^*, K_8^*, K_{12}^*, K_{14}^* and K_{15}^* show some highly irregular behaviour, whereas K_1^*, K_3^*, K_4^*, K_5^* and

L	K_1^*	K_2^*	K_3^*	K_4^*	K_5^*
4	0.107845	0.0905415	0.124834	0.0782122	0.107248
6	0.106912	0.097993		0.0917084	0.106496
8	0.106446	0.100425		0.0964137	0.105555
12	0.104785	0.101524	0.107327	0.0994292	0.104127
16	0.103919	0.101814	0.105460	0.100490	0.103434
24	0.103108	0.101979	0.103876	0.101284	0.102815
32	0.102748	0.102025	0.103221	0.101586	0.102551
64	0.102305	0.102061	0.102456	0.101915	0.102234
128	0.102150	0.102068	0.102200	0.102019	0.102126
256	0.102097	0.102070	0.102113	0.102054	0.102090
∞	0.102065	0.102070	0.102069	0.102068	0.102069
σ	(6)	(1)	(2)	(3)	(3)

TABLE IV: Critical points for fcc; location of, respectively, maximum $\mathcal{C}$, maximum and minimum $\partial\mathcal{C}/\partial K$, maximum and minimum $\partial^2\mathcal{C}/\partial K^2$.

K_6^* seem well-behaved enough. The others have some irregularities but nothing too bad. It is somewhat ironic though that K_8^* and K_{15}^*, being so irregular, also have the lowest error estimates. When calculating the different scaling fits we could not use the same data set on all sequences. Adding a point sometimes wreck the scaling completely, while adding yet another give a reasonable fit again. However, the asymptotic estimates are medians of three different fits that all give acceptable parameters. In Figure 9 the points are shown with fitted curves.

A lower bound on K_c is provided by the sequence K_4^*, and the upper bound by K_2^* since these two seem well-behaved for this purpose. This gives

$$0.369678 \leq K_c \leq 0.369761$$

or $K_c = 0.36972(4)$. Taking the median of the medians, after excluding sequences 7, 8, 12, 14 and 15 gives $K_c = 0.369722$. Since the data set now is rather small and also have a bit of spread, merely taking quartiles to get error estimates is probably a little optimistic. We get a somewhat larger, but safer, error estimate if we instead take the half-width of the set

L	K_6^*	K_7^*	K_8^*	K_9^*	K_{10}^*
4	0.103643	0.0927308	0.0899291	0.0985371	0.0737583
6	0.104514	0.0988013	0.0975338	0.101597	0.0882838
8	0.104396	0.100627	0.0999271	0.102282	0.0937174
12	0.103546	0.101545	0.101213	0.102368	0.0978437
16	0.103076	0.101802	0.101602	0.102311	0.0994393
24	0.102633	0.101961	0.101860	0.102222	0.100711
32	0.102437	0.102010	0.101948	0.102174	0.101217
64	0.102197	0.102055	0.102035	0.102109	0.101790
128	0.102113	0.102066	0.102059	0.102084	0.101978
256	0.102085	0.102069	0.102067	0.102075	0.102041
∞	0.102068	0.102069	0.102068	0.102068	0.102069
σ	(4)	(1)	(2)	(4)	(2)

TABLE V: Critical points for fcc; location of the maximum of, respectively, $\partial\bar{\mu}/\partial K$, $\partial \log \bar{\mu}/\partial K$, $\partial \log \chi/\partial K$, $\bar{\chi}$ and ϕ.

remaining after excluding the extreme points. This gives $K_c = 0.369722(7)$ which misses the remarkably precise estimate $K_c = 0.36973980(9)$ of [19]. Another estimate is $K_c = 0.3697(7)$ from [20]. The critical internal energy is determined as before. Fitting on the six largest lattices gave very convincing curves and resulted in $\mathcal{U}_c = 0.43161(9)$ and for the free energy $\mathcal{F}_c = 0.833356(6)$ which gives the entropy $\mathcal{S}_c = \mathcal{F}_c - 2\,K_c\,\mathcal{U}_c = 0.51421(7)$. From [18] we cite $K_c = 0.369787(15)$, $\mathcal{U}_c = 0.437(3)$ and $\mathcal{S}_c = 0.5103(18)$.

C. Critical values

Next we wish to determine the growth of a number of quantities near K_c. Though all the points in the Tables I to IX correspond to some critical value, not all of them are very important. We will focus on a small selection only, such as the maximum specific heat, susceptibility, Binder cumulant derivative, magnetisation derivative and the magnetisations at this critical point.

For the bcc lattice these values are listed in Table X, for the fcc lattice in Table XI and

L	K^*_{11}	K^*_{12}	K^*_{13}	K^*_{14}	K^*_{15}
4	0.113202	0.0952823	0.122254	0.0888639	
6	0.108848	0.0995775		0.0966066	
8	0.106628	0.100819	0.109308	0.0990016	0.103398
12	0.104570	0.101552	0.105930	0.100644	0.102500
16	0.103683	0.101781	0.104531	0.101218	0.102235
24	0.102932	0.101937	0.103372	0.101648	0.102122
32	0.102621	0.101992	0.102898	0.101810	0.102095
64	0.102256	0.102047	0.102347	0.101987	0.102075
128	0.102132	0.102063	0.102163	0.102043	0.102071
256	0.102091	0.102069	0.102101	0.102061	0.102071
∞	0.102069	0.102070	0.102070	0.102068	0.102071
σ	(1)	(1)	(1)	(2)	(1)

TABLE VI: Critical points for fcc; location of, respectively, the minimum ϕ, the minimum and maximum ψ, the maximum $\partial\mathcal{Q}/\partial K$ and the crossing point where $\mathcal{Q}_L = \mathcal{Q}_{L/2}$.

for the diamond lattice in Table XII.

We intend to compare the three lattices and see if the corresponding growth rates have any substantial differences. Indeed, only the simplest of scaling will be assumed, namely of the type $c_0 + c_1\, L^\lambda$, and it is only the exponent λ that we are interested in.

First, the specific heat maximum. Determining its growth rate turns out to be frustratingly hard to determine in a conclusive way. The result seems very dependent on which data points are included in a fitting procedure. In [13] the growth rate was estimated, and indeed conjectured, to be $\lambda = 1/16$. The procedure used there consisted in first determining the c_0 that gave the least varying slopes of a log-log fit for different data sets. Though useful for getting a quick estimate, it is somewhat too dependent on which of the present data points one uses, and it does not really help in comparing the lattices. Also, the data in [13] were gathered on considerably larger lattices and with a better precision at that, and thus depended less on the chosen data set. For the current lattices we can, simply put, choose data sets for each lattice and obtain more or less the same growth rate. Depending on the

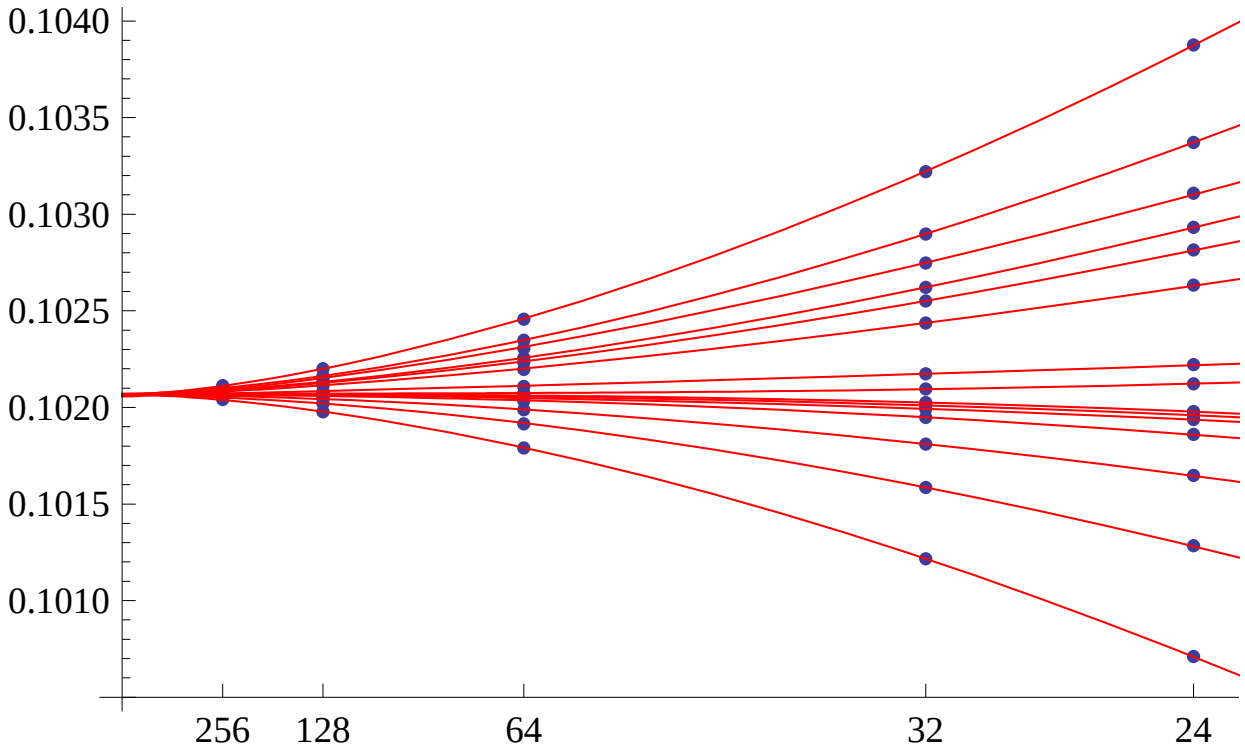

FIG. 8: The critical points $K_1^*, \ldots, K_{15}^*$ vs $1/L$ with fitted curves for the fcc lattice.

chosen data set we can get growth rates between 0.04 and 0.12, a rather wide interval. Any estimate would therefore rely too much on the method. However, we can at least test the conjecture $\lambda = 1/16$ and see how well the lattices fit to such a growth rate when forced. In Figure 10 we have forced $\lambda = 1/16$ upon each lattice and let Mathematica choose the remaining parameters for $L \geq 12$. The result is acceptable enough to fool the eye but of course in no way conclusive.

We move on to the growth rate of the maximum susceptibility, which is considerably easier to deal with. Here we may safely ignore the constant c_0 and therefore estimate λ by using the slope of linear fits to the logarithm of the data. We used data sets of the form $L \geq L_{\min}$ and let $L_{\min} = 12, 16, 24, 32$ for all lattices. The resulting slopes ended up in the

L	K_1^*	K_2^*	K_3^*	K_4^*	K_5^*
4	0.389786	0.359725		0.338343	0.389288
6	0.384395	0.368236	0.399018	0.357310	0.382626
8	0.380750	0.370275	0.389627	0.363365	0.379217
12	0.375688	0.370076	0.379983	0.366493	0.374572
16	0.373881	0.370220	0.376574	0.367902	0.373117
24	0.371890	0.369965	0.373212	0.368777	0.371418
32	0.371147	0.369920	0.371968	0.369167	0.370838
48	0.370478	0.369829	0.370897	0.369434	0.370309
64	0.370248	0.369831	0.370518	0.369576	0.370143
96	0.369989	0.369771	0.370124	0.369640	0.369929
128	0.369900	0.369761	0.369987	0.369678	0.369861
∞	0.369724	0.369717	0.369730	0.369733	0.369721
σ	(25)	(39)	(34)	(12)	(34)

TABLE VII: Critical points for the diamond lattice; location of, respectively, maximum $\mathcal{C}$, maximum and minimum $\partial\mathcal{C}/\partial K$, maximum and minimum $\partial^2\mathcal{C}/\partial K^2$.

following intervals

$$\begin{aligned} \text{sc} \quad & \lambda = 1.988 \pm 0.007 \\ \text{bcc} \quad & \lambda = 1.985 \pm 0.006 \\ \text{fcc} \quad & \lambda = 1.983 \pm 0.004 \\ \text{d} \quad & \lambda = 1.979 \pm 0.007 \end{aligned} \tag{1}$$

where the sc estimate is quoted from [13]. The estimates intersect in $\lambda = 1.984 \pm 0.003$. In Figure 11 we show a log-log plot of the maxima for the bcc, fcc and d lattices together with linear fits.

Next, the growth rate of the maximum derivative of the Binder cumulant. The slopes

L	K_6^*	K_7^*	K_8^*	K_9^*	K_{10}^*
4	0.382836	0.363154	0.358324	0.373538	0.328180
6	0.379415	0.369132	0.367016	0.373888	0.350283
8	0.377248	0.370687	0.369413	0.373634	0.358616
12	0.373580	0.370147	0.369546	0.371597	0.363769
16	0.372518	0.370299	0.369898	0.371284	0.366241
24	0.371102	0.369953	0.369766	0.370421	0.367821
32	0.370638	0.369909	0.369792	0.370205	0.368560
48	0.370202	0.369817	0.369757	0.369972	0.369108
64	0.370079	0.369833	0.369792	0.369939	0.369380
96	0.369894	0.369765	0.369745	0.369816	0.369526
128	0.369840	0.369760	0.369747	0.369792	0.369614
∞	0.369722	0.369716	0.369765	0.369719	0.369736
σ	(35)	(43)	(10)	(40)	(28)

TABLE VIII: Critical points for the diamond lattice; location of the maximum of, respectively, $\partial\bar{\mu}/\partial K$, $\partial \log\bar{\mu}/\partial K$, $\partial \log\chi/\partial K$, $\bar{\chi}$ and ϕ.

were

$$\begin{aligned} \text{sc} \quad & \lambda = 1.610 \pm 0.014 \\ \text{bcc} \quad & \lambda = 1.5844 \pm 0.0007 \\ \text{fcc} \quad & \lambda = 1.593 \pm 0.002 \\ \text{d} \quad & \lambda = 1.590 \pm 0.002 \end{aligned} \tag{2}$$

and this time they do not intersect. The sc lattice seems to be the odd man here with a rather wide error estimate. Figure 12 shows a log-log plot of the maxima together with linear fits.

L	K^*_{11}	K^*_{12}	K^*_{13}	K^*_{14}	K^*_{15}
4		0.366322		0.356151	
6	0.385862	0.369867	0.393300	0.364989	
8	0.381052	0.370975	0.385669	0.367971	0.373156
12	0.375353	0.370161	0.377688	0.368651	0.370271
16	0.373682	0.370332	0.375186	0.369355	0.369964
24	0.371642	0.369931	0.372401	0.369434	0.369816
32	0.370974	0.369892	0.371453	0.369580	0.369693
48	0.370373	0.369807	0.370623	0.369644	0.369743
64	0.370198	0.369830	0.370361	0.369725	0.369793
96	0.369949	0.369760	0.370032	0.369703	0.369737
128	0.369876	0.369758	0.369928	0.369726	0.369724
∞	0.369720	0.369687	0.36972	0.369735	0.369740
σ	(32)	(74)	(34)	(38)	(8)

TABLE IX: Critical points for the diamond lattice; location of, respectively, the minimum ϕ, the minimum and maximum ψ, the maximum $\partial\mathcal{Q}/\partial K$ and the crossing point where $\mathcal{Q}_L = \mathcal{Q}_{L/2}$.

The maximum derivative of the magnetisation gave the slopes

$$\begin{aligned} \text{sc} \quad & \lambda = 1.096 \pm 0.013 \\ \text{bcc} \quad & \lambda = 1.095 \pm 0.010 \\ \text{fcc} \quad & \lambda = 1.091 \pm 0.007 \\ \text{d} \quad & \lambda = 1.092 \pm 0.009 \end{aligned} \tag{3}$$

which intersect in the interval 1.092 ± 0.007. See Figure 13 for a log-log plot of the points.

Finally, the value of the magnetisation at the point that gives maximum derivative. The slopes were

$$\begin{aligned} \text{sc} \quad & \lambda = -0.512 \pm 0.012 \\ \text{bcc} \quad & \lambda = -0.496 \pm 0.006 \\ \text{fcc} \quad & \lambda = -0.503 \pm 0.005 \\ \text{d} \quad & \lambda = -0.503 \pm 0.006 \end{aligned} \tag{4}$$

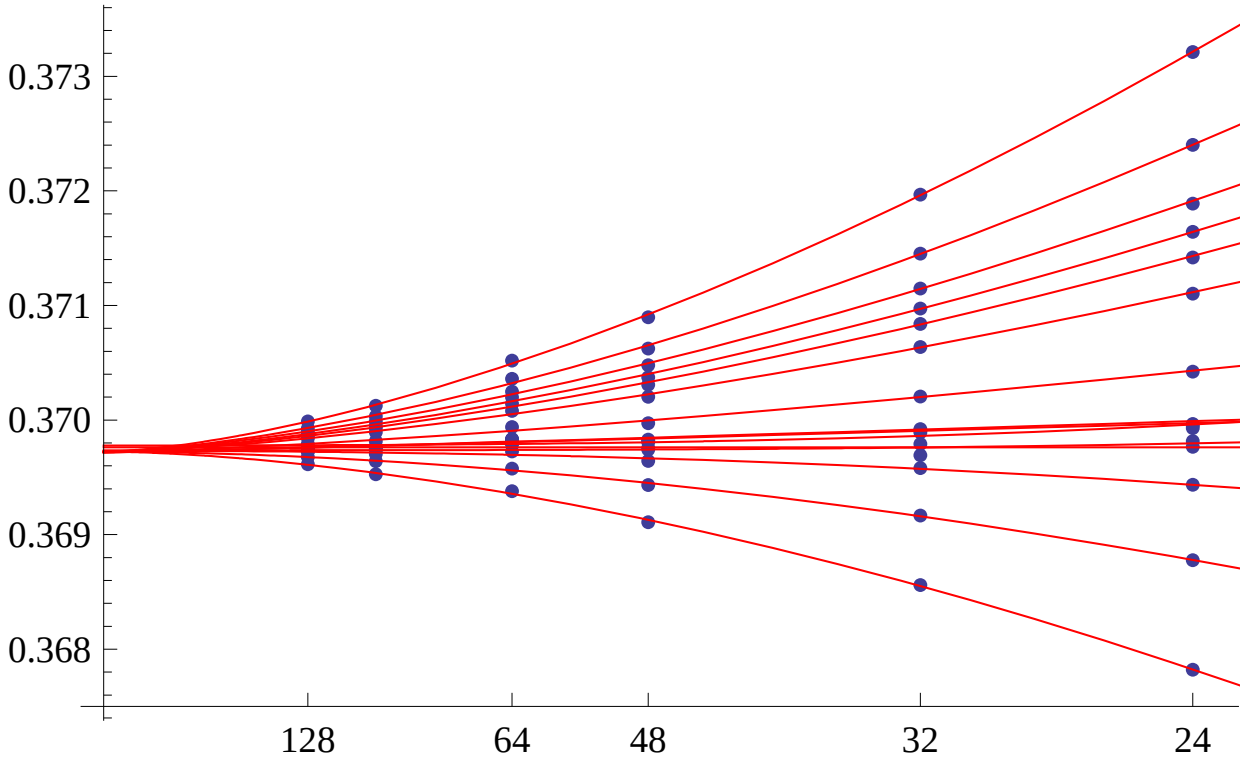

FIG. 9: The critical points $K_1^*, \ldots, K_{15}^*$ vs $1/L$ with fitted curves for the diamond lattice.

and they intersect in the interval -0.501 ± 0.001. Admittedly, it is very tempting to conjecture that this should be $-1/2$. See Figure 14 for a log-log plot of the points.

D. Critical exponents

We intend here to give rough estimates of the critical exponents α, α', β, γ, γ' and δ. It has become the order of the day to assume that $\alpha = \alpha'$ and $\gamma = \gamma'$ but one point of the present study is to test this hypothesis. First we ask the reader to recall the definition of the exponents. The growth of the specific heat near K_c is determined by α, α'

$$\begin{aligned} \alpha &= \lim_{K \to K_c^-} \lim_{L \to \infty} \frac{-\log \mathcal{C}_L(K)}{\log |K - K_c|} \\ \alpha' &= \lim_{K \to K_c^+} \lim_{L \to \infty} \frac{-\log \mathcal{C}_L(K)}{\log |K - K_c|} \end{aligned} \tag{5}$$

L	$\mathcal{C}$	$\bar{\chi}$	$\mathcal{Q}'$	$\bar{\mu}'$	$\bar{\mu}^*$
4	7.103	1.303	5.089	5.750	0.6202
6	10.07	3.119	9.034	10.25	0.5661
8	12.41	5.743	13.98	15.09	0.5166
12	15.96	13.36	26.35	25.25	0.4439
16	18.44	24.07	41.48	35.68	0.3928
24	21.85	54.60	78.82	57.01	0.3264
32	24.27	97.21	124.5	78.85	0.2846
48	27.62	217.5	235.8	123.3	0.2332
64	30.08	385.1	373.0	169.0	0.2019
96	33.72	859.1	705.3	263.0	0.1648
128	36.43	1517.	1113.	358.5	0.1427
192	40.34	3381.	2119.	556.1	0.1157
256	43.12	5959.	3373.	751.2	0.1004

TABLE X: Extreme values for the bcc lattice; maximum of, respectively, $\mathcal{C}$, $\bar{\chi}$, $\partial\mathcal{Q}/\partial K$, $\partial\bar{\mu}/\partial K$ and the value that $\bar{\mu}$ takes at this point.

the susceptibility by γ, γ'

$$\begin{aligned} \gamma &= \lim_{K\to K_c^-} \lim_{L\to\infty} \frac{-\log \bar{\chi}_L(K)}{\log|K-K_c|} \\ \gamma' &= \lim_{K\to K_c^+} \lim_{L\to\infty} \frac{-\log \bar{\chi}_L(K)}{\log|K-K_c|} \end{aligned} \tag{6}$$

the magnetisation by β

$$\beta = \lim_{K\to K_c^+} \lim_{L\to\infty} \frac{\log \bar{\mu}_L(K)}{\log|K-K_c|} \tag{7}$$

and at K_c the exponent δ determines how the magnetisation depends on the external field

$$\frac{1}{\delta} = \lim_{H\to 0^+} \lim_{L\to\infty} \frac{\log \mu_L(K_c, H)}{\log H} \tag{8}$$

The reader should note the order of the limits, that is, first we need data for the asymptotic lattice, then we let K approach K_c or H approach 0. Obviously we cannot do this so we have settled for the same approach as used in [13]. This means that we study the slopes of log-log plots of the quantities near, but not too near, K_c. We have stopped at a distance

L	$\mathcal{C}$	$\bar{\chi}$	$\mathcal{Q}'$	$\bar{\mu}'$	$\bar{\mu}^*$
4	13.56	2.124	10.69	12.22	0.5898
6	17.94	4.992	19.67	20.93	0.5148
8	22.62	9.161	30.72	30.95	0.4720
12	28.09	21.04	58.17	50.71	0.3990
16	31.91	37.67	91.69	70.93	0.3506
24	37.20	84.97	174.3	112.3	0.2895
32	40.96	150.8	275.3	154.6	0.2516
64	50.22	596.4	827.1	329.9	0.1779
128	60.16	2341.	2491.	696.9	0.1249
256	71.35	9252.	7590.	1473.	0.08752

TABLE XI: Extreme values for the fcc lattice; maximum of, respectively, $\mathcal{C}$, $\bar{\chi}$, $\partial\mathcal{Q}/\partial K$, $\partial\bar{\mu}/\partial K$ and the value that $\bar{\mu}$ takes at this point.

L	$\mathcal{C}$	$\bar{\chi}$	$\mathcal{Q}'$	$\bar{\mu}'$	$\bar{\mu}^*$
4	4.602	7.079	5.860	6.795	0.5594
6	6.031	16.84	11.21	11.75	0.4886
8	7.052	31.41	17.65	16.92	0.4399
12	8.504	70.82	33.84	27.44	0.3666
16	9.482	132.3	53.00	38.32	0.3252
24	10.87	286.8	102.2	60.35	0.2645
32	11.87	512.2	161.5	83.18	0.2302
48	13.24	1134.	306.4	129.1	0.1875
64	14.35	2123.	479.6	178.3	0.1651
96	15.75	4427.	918.1	272.1	0.1317
128	16.92	7931.	1468.	374.4	0.1137

TABLE XII: Extreme values for the diamond lattice; maximum of, respectively, $\mathcal{C}$, $\bar{\chi}$, $\partial\mathcal{Q}/\partial K$, $\partial\bar{\mu}/\partial K$ and the value that $\bar{\mu}$ takes at this point.

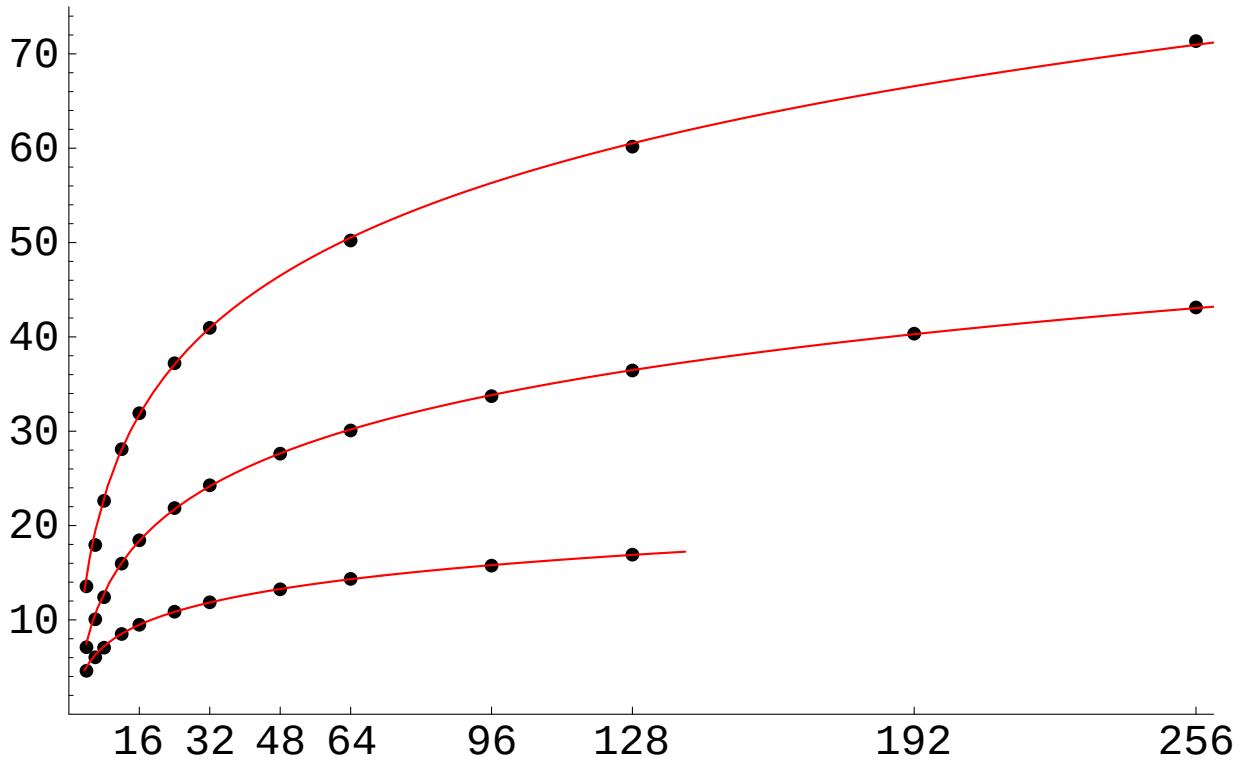

FIG. 10: Maximum specific heat $\mathcal{C}$ vs L for the fcc, bcc and diamond lattice (downwards). The fitted curves are of type $c_0 + c_1\, L^{1/16}$.

from K_c corresponding to the coupling where at most 1% of the energy distribution spills over U_c. This is shown in the plots below. First, in Figure 15 we see $\log \mathcal{C}_L(K)$ plotted versus $\log|K - K_c|$ for $K < K_c$ and $K > K_c$. Then, in Figure 16 we see $\log \bar{\chi}_L(K)$ versus $\log|K - K_c|$. Finally, in the left panel of Figure 17 $\log \bar{\mu}_L(K)$ versus $\log|K - K_c|$ is shown and the right panel shows $\log \mu_L(K_c, H)$ versus $\log H$, so that the slope measures $1/\delta$. Also, we have not been able to gather data for this purpose for lattices of all linear orders since they require too much computer memory during sampling. Thus we only have these data for $L \leq 48$ in the bcc case and for $L \leq 24$ in the fcc and diamond case. Note that we use μ rather than $\bar{\mu}$ when measuring δ. In passing, the magnetisation μ has the properties $\mu_L(K, 0) = 0$ for all K and $\mu_L(K, H) = -\mu_L(K, -H)$ whereas $\bar{\mu}_L(K, H) > 0$ for all K, H and finite L but $\lim_{L\to\infty} \bar{\mu}_L(K, 0) = 0$ for $K < K_c$. We assume as an axiom that

$$\lim_{H\to 0^+} \lim_{L\to\infty} \mu_L(K, H) = \lim_{L\to\infty} \bar{\mu}_L(K)$$

As the attentive reader surely recognises, the order of the limits on the left-hand side matters.

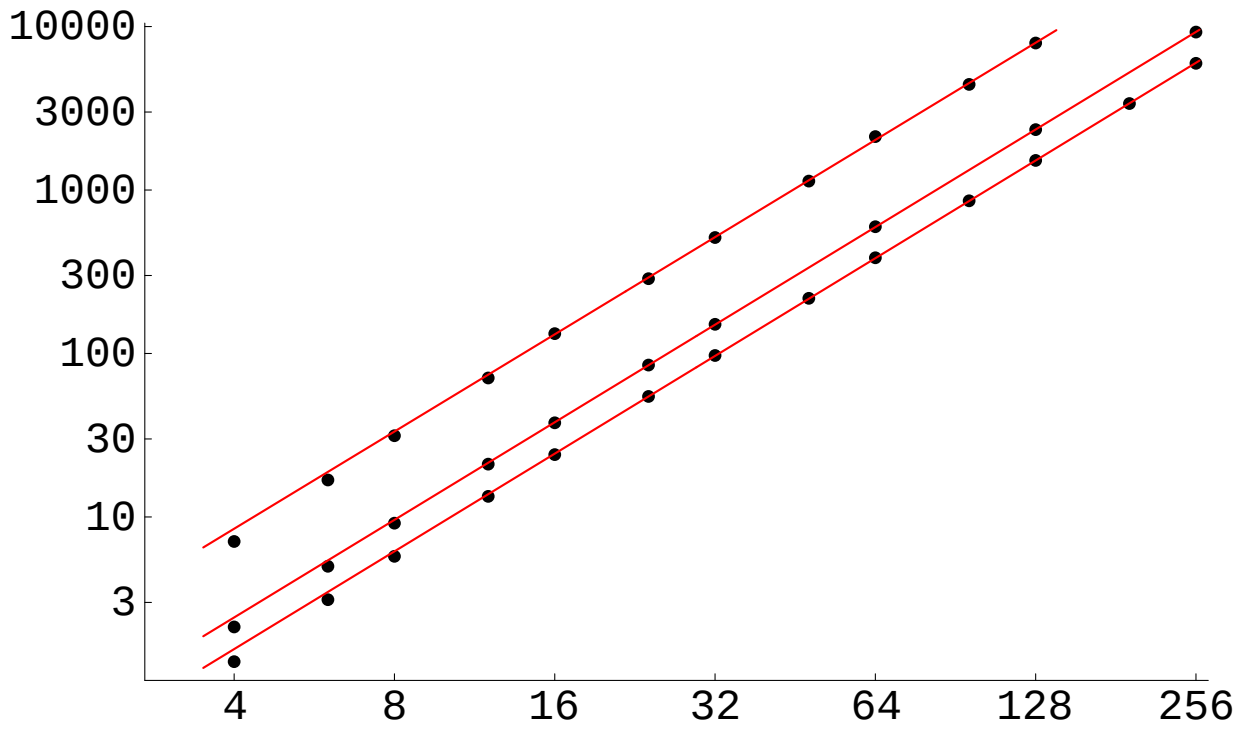

FIG. 11: Logarithm of maximum susceptibility $\log \bar{\chi}$ vs $\log L$ for the diamond, fcc and bcc lattice (downwards).

As is clearly seen in these pictures is that the curves line up in a rather convincing way, and the asymptotic slope of these curves is our desired exponent. Using only our eyes to fit a straight line we obtained the following rough estimates

$$\begin{aligned} \text{sc} \quad & \alpha = 0.22 \pm 0.015 \\ \text{bcc} \quad & \alpha = 0.275 \pm 0.025 \\ \text{fcc} \quad & \alpha = 0.27 \pm 0.02 \\ \text{d} \quad & \alpha = 0.26 \pm 0.02 \end{aligned} \tag{9}$$

Clearly, our current estimates are considerably higher than the one for sc given in [13]. However, as can be seen in Figure 15, the curves are slow to straighten up into a line and this makes it particularly difficult to make a good estimate of this exponent. Again, our present data probably suffers from relying on too small lattices due to the very slow growth rate of the specific heat. However, the curves are better fitted with a straight line for α'

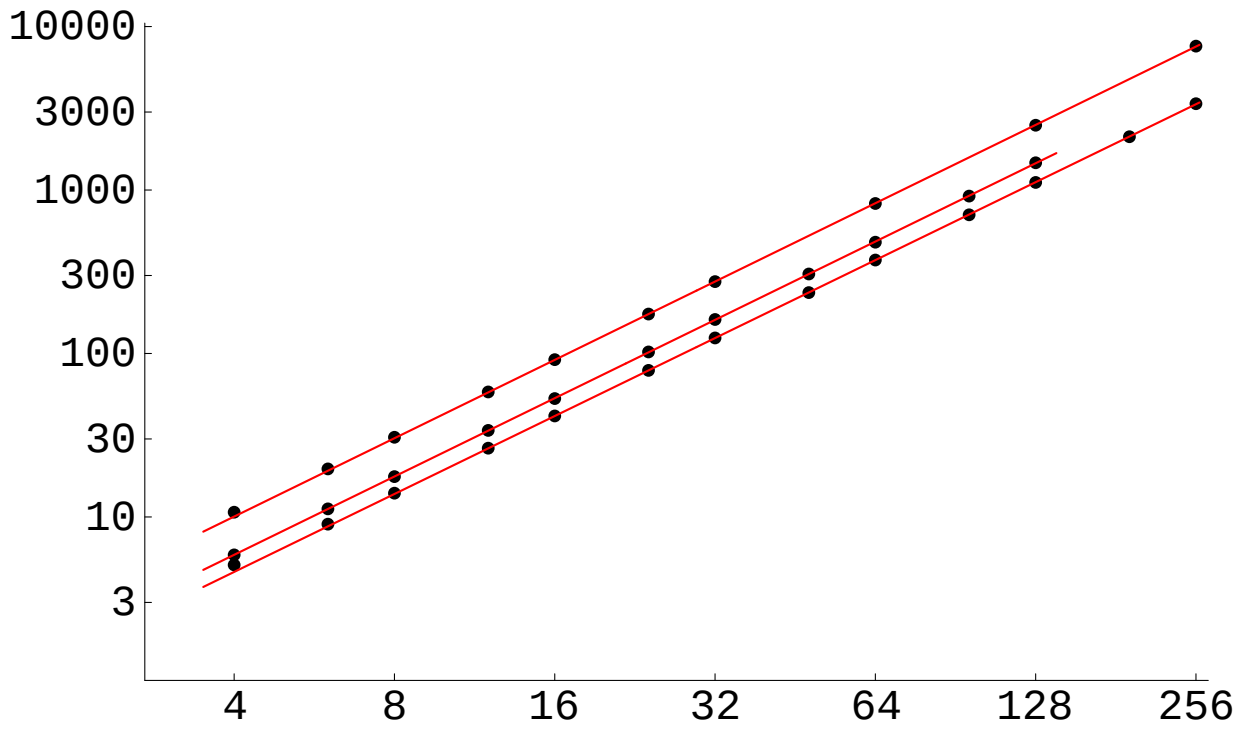

FIG. 12: Logarithm of maximum derivative of the Binder cumulant $\log \partial \mathcal{Q}/\partial K$ vs $\log L$ for the fcc, diamond and bcc lattice (downwards).

though, which we estimate to be

$$\begin{aligned} \text{sc} \quad & \alpha' = 0.164 \pm 0.007 \\ \text{bcc} \quad & \alpha' = 0.177 \pm 0.012 \\ \text{fcc} \quad & \alpha' = 0.17 \pm 0.02 \\ \text{d} \quad & \alpha' = 0.187 \pm 0.013 \end{aligned} \tag{10}$$

These compare rather well except possibly for the diamond lattice. Though the intervals do not intersect, their union is comparatively narrow, 0.175 ± 0.025. Traditional values of α (and α') are close to 0.11–0.12, see Table XX for comparison, though in [21] the authors obtained the value $\alpha \approx 0.18$.

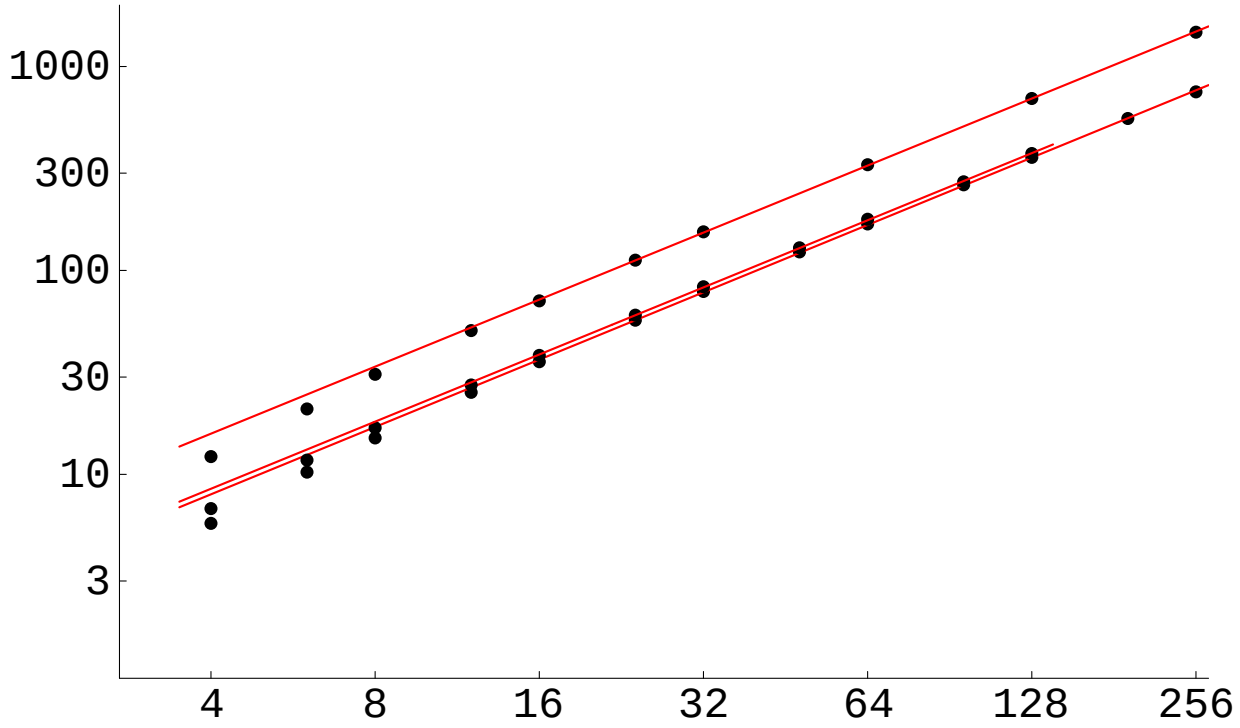

FIG. 13: Logarithm of maximum derivative of the magnetisation $\log \partial\bar{\mu}/\partial K$ vs $\log L$ for the fcc, diamond and bcc lattice (downwards).

For γ we get the estimates

$$\begin{aligned} \text{sc} \quad & \gamma = 1.205 \pm 0.025 \\ \text{bcc} \quad & \gamma = 1.23 \pm 0.015 \\ \text{fcc} \quad & \gamma = 1.24 \pm 0.02 \\ \text{d} \quad & \gamma = 1.225 \pm 0.025 \end{aligned} \tag{11}$$

which actually agrees in the interval 1.225 ± 0.005. For γ' we get

$$\begin{aligned} \text{sc} \quad & \gamma' = 1.265 \pm 0.015 \\ \text{bcc} \quad & \gamma' = 1.285 \pm 0.04 \\ \text{fcc} \quad & \gamma' = 1.26 \pm 0.02 \\ \text{d} \quad & \gamma' = 1.32 \pm 0.06 \end{aligned} \tag{12}$$

and they also intersect, this time in 1.27 ± 0.01. Typically γ (and γ') are estimated to be close to 1.24, see Table XX. This is actually right between our estimates of γ and γ'.

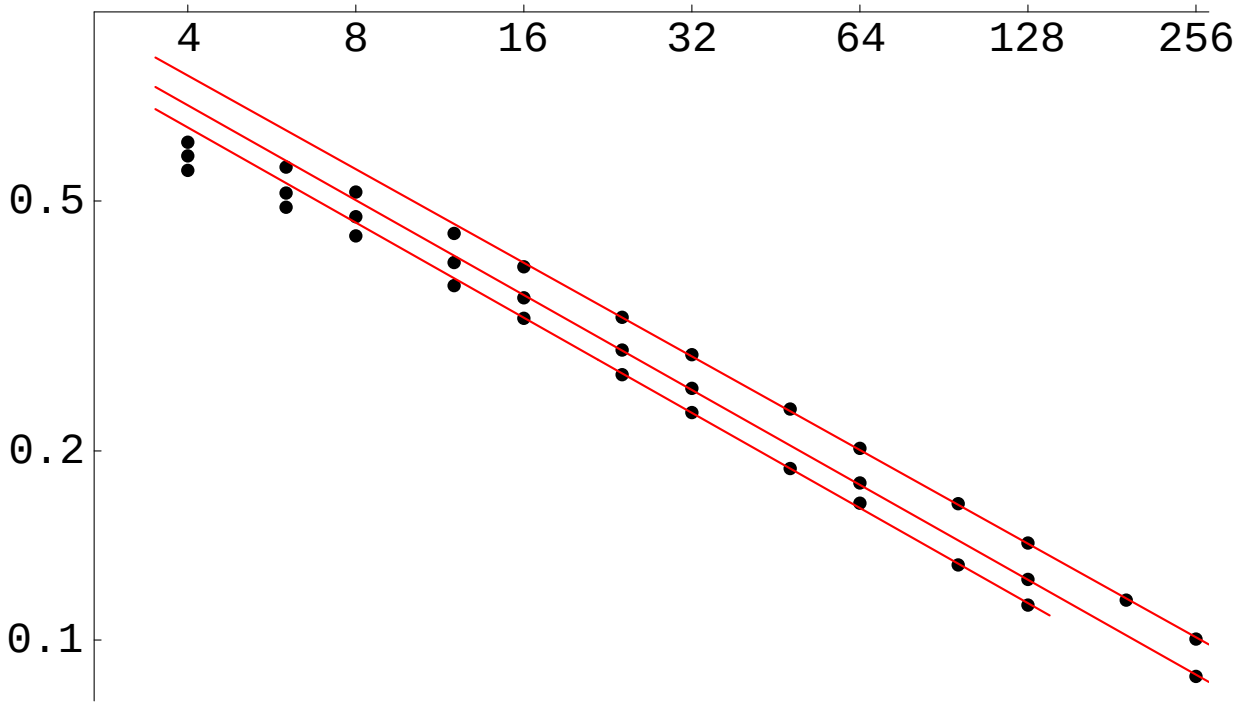

FIG. 14: Logarithm of the magnetisation $\log \bar{\mu}^*$ vs $\log L$ at the critical point for the bcc, fcc and diamond lattice (downwards).

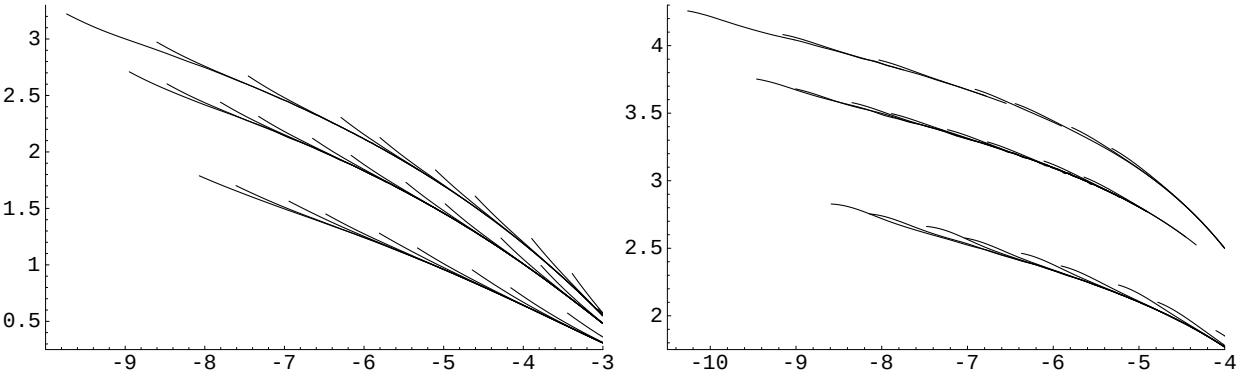

FIG. 15: $\log \mathcal{C}$ vs $\log |K - K_c|$ for $K < K_c$ (left) and $K > K_c$ (right) for the fcc, bcc and diamond lattice (downwards) and all linear orders.

For the exponent β we estimated

$$\begin{aligned} \text{sc} \quad & \beta = 0.323 \pm 0.008 \\ \text{bcc} \quad & \beta = 0.325 \pm 0.008 \\ \text{fcc} \quad & \beta = 0.325 \pm 0.002 \\ \text{d} \quad & \beta = 0.33 \pm 0.01 \end{aligned} \tag{13}$$

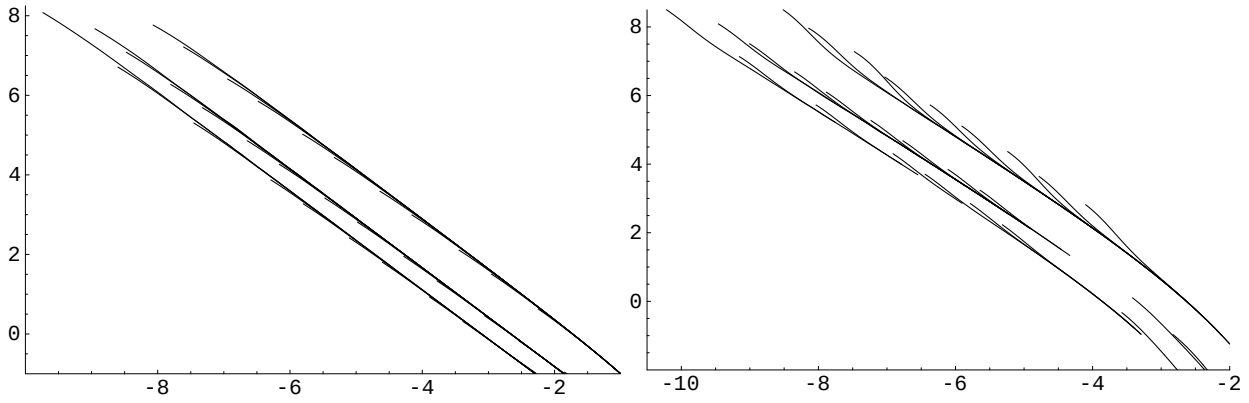

FIG. 16: $\log \bar{\chi}$ vs $\log |K - K_c|$ for $K < K_c$ (left) and $K > K_c$ (right) for the diamond, bcc and fcc lattice (downwards) and all linear orders.

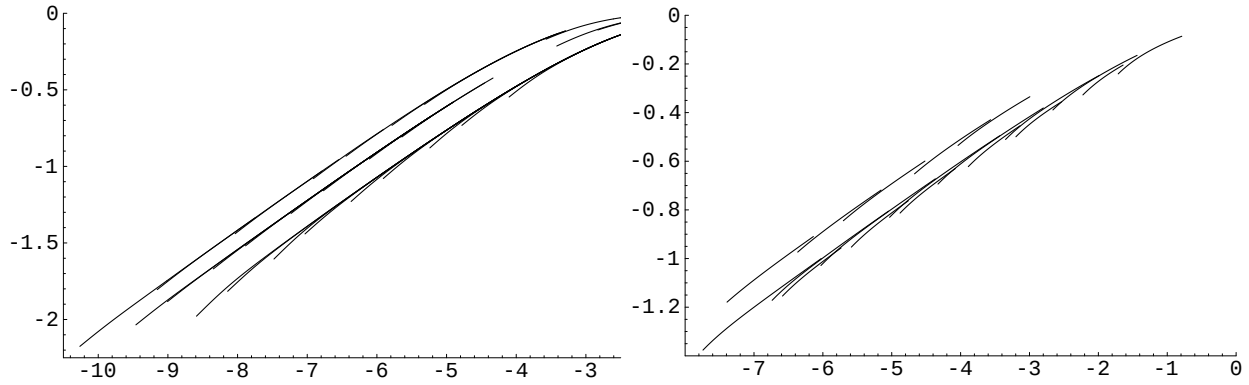

FIG. 17: Left: $\log \bar{\mu}$ vs $\log |K - K_c|$ for $K > K_c$ for the fcc, bcc and diamond lattice (downwards) and all linear orders. Right: $\log \mu(K_c, H)$ vs $\log H$ for $H > 0$ for the diamond, bcc and fcc lattice (downwards, though bcc and fcc are almost indistinguishable).

which intersect in 0.325 ± 0.002. This is actually very close to the traditional estimates of β, such as those listed in Table XX. Finally, for the exponent δ we estimated

$$\begin{aligned} \text{sc} \quad & 1/\delta = 0.205 \pm 0.001 \\ \text{bcc} \quad & 1/\delta = 0.203 \pm 0.004 \\ \text{fcc} \quad & 1/\delta = 0.200 \pm 0.004 \\ \text{d} \quad & 1/\delta = 0.195 \pm 0.004 \end{aligned} \tag{14}$$

The intervals for sc, bcc and fcc overlap in 0.204 (corresponding to $\delta \approx 4.90$), though barely, but the diamond lattice remains faithful to its habit of being the odd one out. However, this is more likely a result of that we cannot get very close to $H = 0$ for such small lattice orders. The authors of [10] give $\delta = 4.7893(8)$ from which we then deviate in the first

decimal, see also Table XX.

IV. COMBINATORIAL QUANTITIES

A. Plots

As the reader noticed in Figures 1 and 2 there was no clear difference between the different lattices in the behaviour of the specific heat. The combinatorial quantities are a little more discriminating however. The function $K(U)$ does not have any interesting behaviour (in short, $K(0) = 0$ and $K(U_c) \to K_c$ as $L \to \infty$ and then $K(U) \to \infty$ as $U \to \infty$) so let us first show the derivative $\partial K/\partial U$ for the different lattices. These are shown in Figures 18 and 19. Roughly, this quantity's behaviour is the inverse of the specific heat's; near K_c the specific heat goes to infinity and $\partial K/\partial U$ goes to zero near U_c, this is all worked out in detail in [14]. Though the different lattices have a clearly different behaviour on a global scale, in this case for $0 \leq U \leq 2\,U_c$, they do not differ particularly when observed very close to U_c, as the inset pictures show for $0.9\,U_c \leq U \leq 1.1\,U_c$.

However, the diamond lattice has a peculiar feature in that it displays a very small local maximum, as the second inset picture clearly demonstrates. The series expansion, obtained from [22], is included in the picture (red curve). From the expansion formula, a 16 degree polynomial, we find the maximum located at $U \approx 0.127588$ with the value $\partial K/\partial U \approx 1.00828$. Since the series expansion of $\partial K/\partial U$ corresponds to the inverse specific heat of an infinite diamond lattice we can easily obtain the location and value of the minimum in the specific heat. These were stated in Section III A.

We move on to the next derivative, $\partial^2 K/\partial U^2$, shown in Figures 20 and 21. The data gets more noisy, but are fairly good where it matters, near U_c. We wish only to demonstrate the general behaviour, so the figures only show plots for $12 \leq L \leq 64$. It should be clear however, that near U_c we first see a very sharp and quickly growing minimum followed by a rather slower growing maximum.

Note that $K(U)$ is an odd function for bipartite lattices. The fcc is not bipartite though. This exception is clearly demonstrated by the second derivative for fcc, which is asymptotically -8 at $U = 0$, whereas the others are asymptotically 0. The second derivative for the bcc lattice also demonstrates other interesting features, such as a local minimum at $U \approx 0.1$

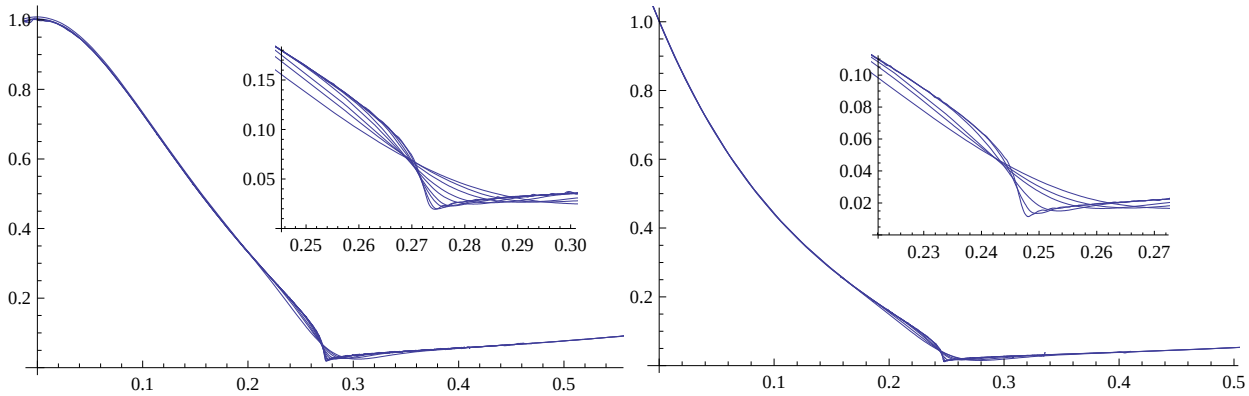

FIG. 18: $\partial K/\partial U$ vs energy U, $-1 \leq \epsilon \leq 1$ and inset $-0.1 \leq \epsilon \leq 0.1$, for the bcc (left) and fcc (right) lattice. Lattice sizes $16 \leq L \leq 256$ and $16 \leq L \leq 256$ respectively.

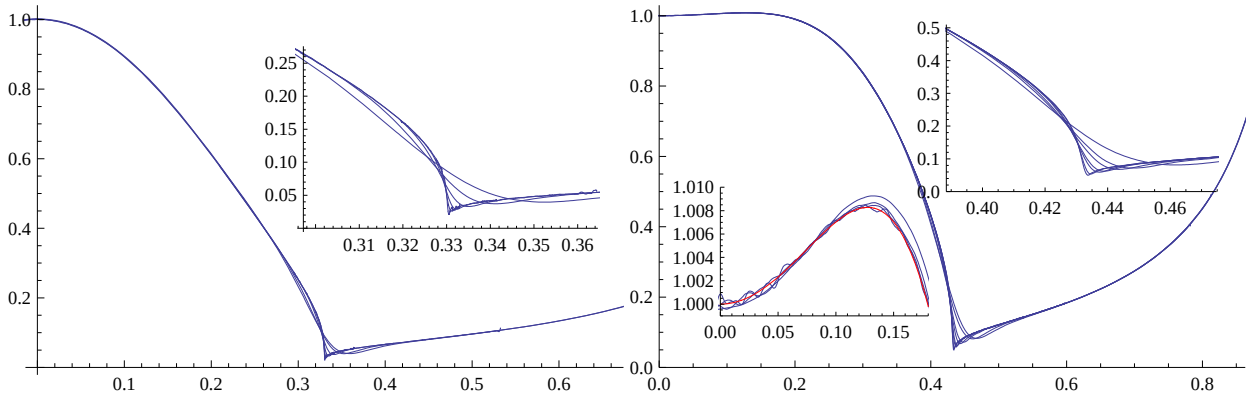

FIG. 19: $\partial K/\partial U$ vs energy U, $-1 \leq \epsilon \leq 1$ and inset $-0.1 \leq \epsilon \leq 0.1$, for the sc (left) and d (right) lattice. Lattice sizes $16 \leq L \leq 512$ and $16 \leq L \leq 128$ respectively. Second inset for d lattice shows series expansion (red) and data for $L = 8, 12, 16, 24$.

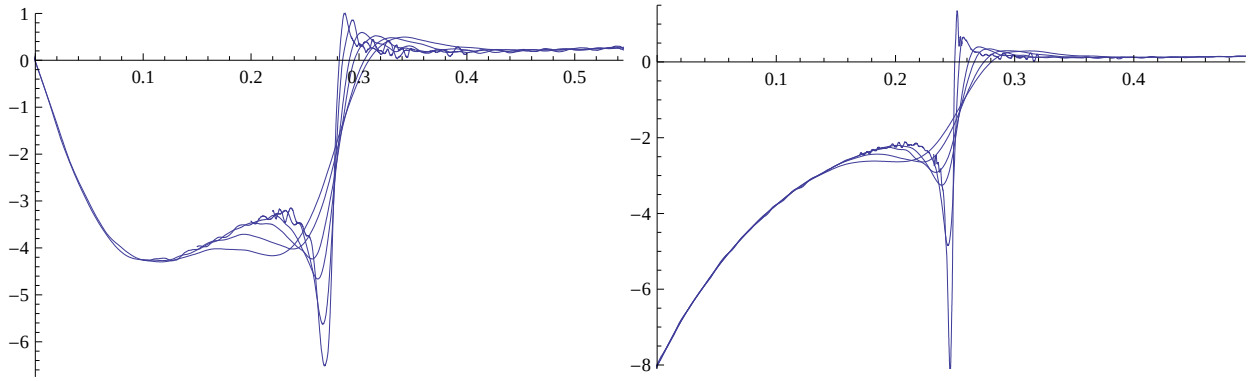

FIG. 20: $\partial^2 K/\partial U^2$ vs energy U, $-1 \leq \epsilon \leq 1$, for the bcc (left) and fcc (right) lattice. Lattice sizes $12 \leq L \leq 64$ and $12 \leq L \leq 128$ respectively.

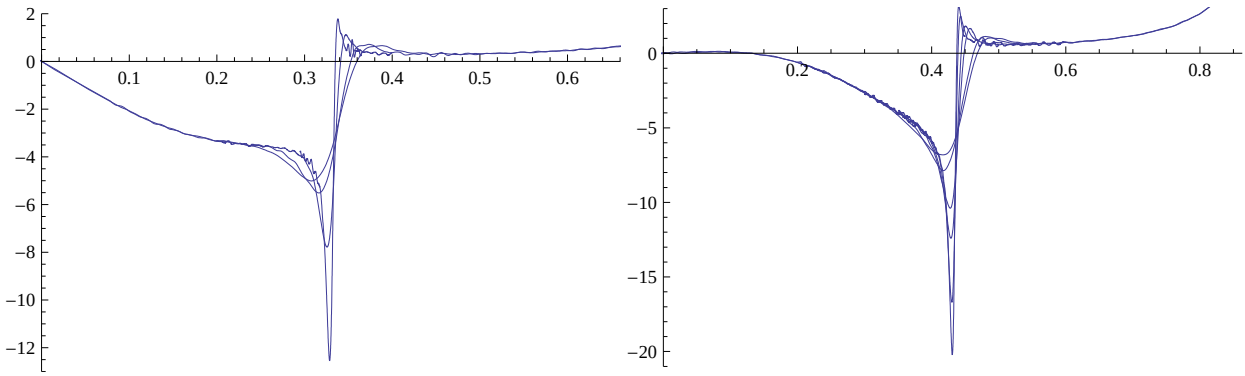

FIG. 21: $\partial^2 K/\partial U^2$ vs energy U, $-1 \leq \epsilon \leq 1$, for the sc (left) and d (right) lattice. Lattice sizes $12 \leq L \leq 64$.

followed by a local maximum at $U \approx 0.22$; these are both absent from the sc lattice.

B. Critical points and values

In section III C we determined the growth rates for a number of quantities. Here we will do the same for their energy dependent counterparts. In Tables XIII, XIV and XV we list a few points and values of interest, related to the function $K(U)$. Note that the derivative of $K(U)$ corresponds roughly to the incerse of the specific heat, see [14]. The minimum should thus go to zero as $L \to \infty$. The location of the minimum should approach U_c and the value of $K(U^*)$ should approach K_c. It is far from clear however at what rate these points and values scale, but we will at least plot their behaviour. These properties generally require very large lattices for any scaling to be convincing. The finite size effects are at times rather large. Thus, we had to leave out $L = 4$ in the bcc case. Also, the second minimum of $\partial^2 K/\partial U^2$ does not even exist for $L \leq 8$.

In the left plot of Figure 22 it is shown how $\log(U^* - U_c)$ behaves for the three lattices. Needless to say, the linear fit is not entirely convincing since the lattices are too small. Possibly, one might claim that the fcc lattice deviates a little from the other two. A similar plot for the sc lattice would give a slightly steeper slope, but even for those considerably larger lattices the linearity is not entirely satisfactory yet. Alas, this quantity requires huge lattices. A similar statement holds for $\log(K(U^*) - K_c)$, see right plot of Figure 22.

The situation is largely the same for the minimum of $\partial K/\partial U$. In the left picture of Figure 23 we see the logarithm of the minimum for the three lattices. The fitted lines all

L	U^*	K'	K	$-K''$
6	0.27171	-0.06966	0.160988	8.231
8	0.30304	-0.006133	0.159465	5.109
12	0.30885	0.01912	0.158921	4.166
16	0.30442	0.02431	0.158579	4.013
24	0.29644	0.02624	0.158169	4.232
32	0.29108	0.02628	0.157945	4.658
48	0.28509	0.02568	0.157720	5.628
64	0.28134	0.02439	0.157598	6.508
96	0.27806	0.02278	0.157502	8.910
128	0.27656	0.02192	0.157461	10.39
192	0.27508	0.01969	0.157422	13.94
256	0.27426	0.01920	0.157404	18.40

TABLE XIII: Critical points and values for the bcc lattice; location U^* of the minimum of $\partial K/\partial U$, value of the minimum $\partial K/\partial U$, value of K at U^*, minimum of $\partial^2 K/\partial U^2$.

L	U^*	K'	K	$-K''$
6	0.27857	-0.006924	0.103651	
8	0.28469	0.007812	0.103270	
12	0.28050	0.01483	0.102917	2.636
16	0.27459	0.01636	0.102700	2.641
24	0.26661	0.01671	0.102471	2.917
32	0.26110	0.01649	0.102337	3.252
64	0.25342	0.01497	0.102174	4.844
128	0.24975	0.01328	0.102109	8.231
256	0.24819	0.01157	0.102086	13.99

TABLE XIV: Critical points and values for the fcc lattice; location U^* of the minimum of $\partial K/\partial U$, value of the minimum $\partial K/\partial U$, value of K at U^*, minimum of $\partial^2 K/\partial U^2$.

L	U^*	K'	K	$-K''$
4	0.55647	0.1024	0.385308	4.713
6	0.50739	0.09248	0.378986	4.889
8	0.49425	0.09195	0.377049	5.295
12	0.46904	0.08259	0.373450	6.814
16	0.46225	0.08149	0.372573	7.862
24	0.44853	0.07157	0.371108	10.37
32	0.44373	0.06768	0.370649	12.41
48	0.43909	0.06210	0.370233	16.69
64	0.43754	0.05917	0.370112	20.19
96	0.43471	0.05361	0.369905	30.16
128	0.43378	0.05047	0.369845	40.93

TABLE XV: Critical points and values for the diamond lattice; location U^* of the minimum of $\partial K/\partial U$, value of the minimum $\partial K/\partial U$, value of K at U^*, minimum of $\partial^2 K/\partial U^2$.

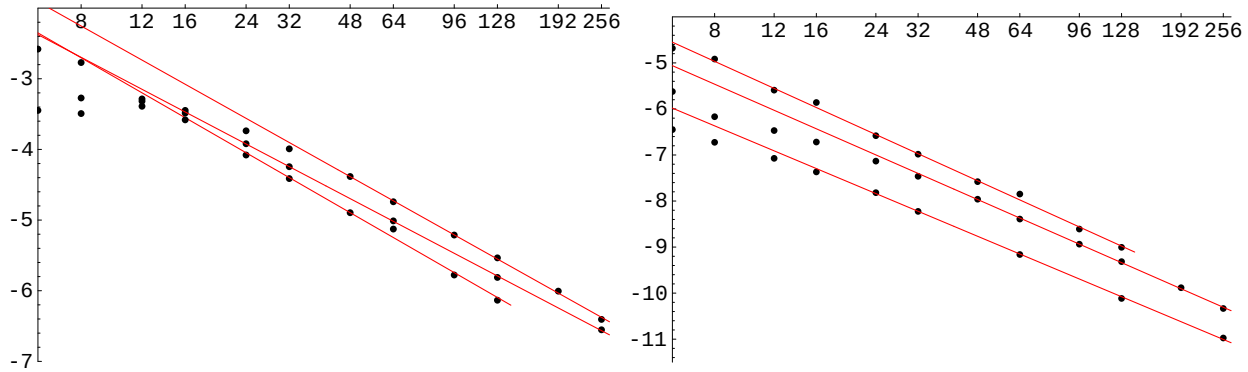

FIG. 22: Left: $\log(U^* - U_c)$ vs $\log L$ for the bcc, fcc and diamond lattice (downwards), where U^* is the location of the minimum $\partial K/\partial U$. Right: $\log(K(U^*) - K_c)$ vs $\log L$ for the diamond, bcc and fcc lattice (downwards).

have a slope of roughly 0.2, the same as for sc in [13], though the bcc and fcc suffer heavily from finite size effects. The diamond lattice does not seem to do that, however. This could perhaps be an effect of its helical boundary conditions.

The right plot shows the logarithm of the absolute value of the minimum second derivative of K, ie $\log|\min \partial^2 K/\partial U^2|$ versus $\log L$. As usual the finite size effects are pervasive, though

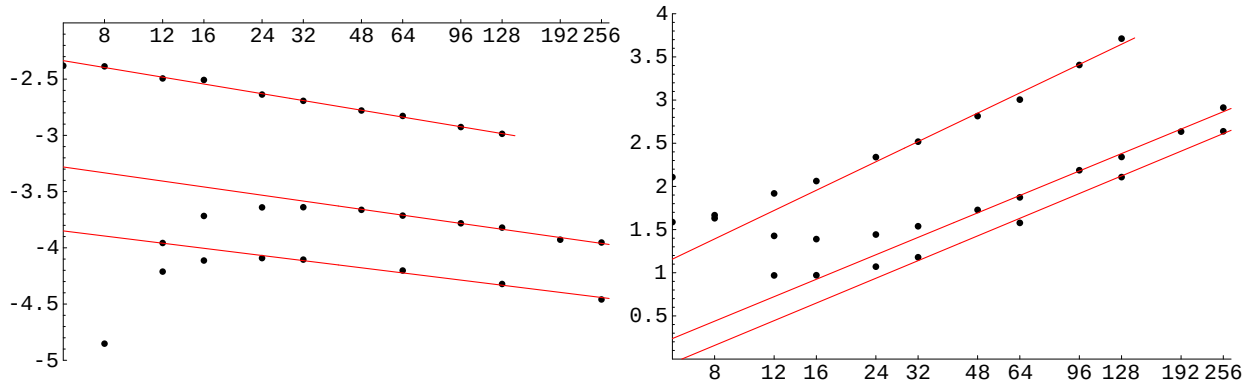

FIG. 23: Left: $\log \min \partial K/\partial U$ vs $\log L$ for the diamond, bcc and fcc lattice (downwards). Right: $\log |\min \partial^2 K/\partial U^2|$ vs $\log L$ for the diamond, bcc and fcc lattice (downwards).

the diamond lattice seems to have a clearly greater slope, around 0.85 and the other two around 0.70. Actually, in [13] we learned that the sc lattice also seems to prefer a value near 0.85, though the error margins were rather large. We will return to the $\partial K/\partial U$-function a little later.

We look instead at statistical moments of the magnetisation as a function of energy. Here scaling is convincing enough for us to make actual estimates. First the data. In Table XVI, XVII and XVIII some values of interest are listed.

Let us try to estimate the growth rates of these quantities as we did in Section III C. In the left part of Figure 24 we see that the log-log plot of the maximum susceptibility gives a very nice linear behaviour and we estimate the growth exponent as

$$\begin{aligned} \text{sc} \quad & \lambda = 2.06 \pm 0.03 \\ \text{bcc} \quad & \lambda = 2.09 \pm 0.02 \\ \text{fcc} \quad & \lambda = 2.08 \pm 0.02 \\ \text{d} \quad & \lambda = 2.05 \pm 0.02 \end{aligned} \tag{15}$$

which intersect in $\lambda = 2.07$. As before the exponent for sc is taken from [13]. Next, the maximum derivative of the Binder cumulant $Q = 1 - \langle M^4 \rangle / 3 \langle M^2 \rangle^2$. The right part of Figure 24 shows a log-log plot of this and goes well with a linear fit. Slopes were

$$\begin{aligned} \text{sc} \quad & \lambda = 1.26 \pm 0.02 \\ \text{bcc} \quad & \lambda = 1.24 \pm 0.02 \\ \text{fcc} \quad & \lambda = 1.26 \pm 0.03 \\ \text{d} \quad & \lambda = 1.29 \pm 0.01 \end{aligned} \tag{16}$$

L	$\bar{\chi}$	Q'	$\bar{\mu}'$	$\bar{\mu}^*$
6	0.7455	2.386	1.886	0.3350
8	1.687	2.541	2.050	0.3292
12	4.720	3.508	2.536	0.2968
16	9.346	4.646	3.020	0.2694
24	23.51	7.136	3.939	0.2316
32	44.43	9.900	4.821	0.2055
48	105.9	15.95	6.462	0.1721
64	195.3	22.68	8.103	0.1516
96	455.0	37.01	11.07	0.1258
128	828.0	53.94	13.75	0.1099
192	1915.	86.93	18.99	0.09170
256	3458.	130.8	24.10	0.07835

TABLE XVI: Critical values for the bcc lattice; maximum of $\bar{\chi}(U)$, $\partial Q/\partial U$, $\partial \bar{\mu}/\partial U$ and the value that $\bar{\mu}$ takes at this point.

L	$\bar{\chi}$	Q'	$\bar{\mu}'$	$\bar{\mu}^*$
6	1.390	2.341	1.929	0.3286
8	2.962	2.924	2.226	0.3081
12	7.947	4.315	2.839	0.2710
16	15.44	5.824	3.415	0.2443
24	38.18	9.190	4.532	0.2074
32	71.40	12.80	5.557	0.1837
64	309.1	29.65	9.373	0.1345
128	1297.	71.36	16.09	0.09695
256	5399.	178.2	28.34	0.06936

TABLE XVII: Critical values for the fcc lattice; maximum of $\bar{\chi}(U)$, $\partial Q/\partial U$, $\partial \bar{\mu}/\partial U$ and the value that $\bar{\mu}$ takes at this point.

L	$\bar{\chi}$	Q'	$\bar{\mu}'$	$\bar{\mu}^*$
4	3.109	1.880	1.964	0.4638
6	7.776	2.883	2.687	0.3848
8	15.46	3.877	3.276	0.3491
12	35.76	6.486	4.432	0.2863
16	71.62	8.672	5.312	0.2626
24	156.1	15.21	7.500	0.2094
32	287.0	21.78	9.440	0.1834
48	651.8	36.72	13.06	0.1506
64	1287.	50.25	16.02	0.1369
96	2654.	91.41	22.85	0.1072
128	4823.	130.4	29.25	0.09321

TABLE XVIII: Critical values for the diamond lattice; maximum of $\bar{\chi}(U)$, $\partial Q/\partial U$, $\partial\bar{\mu}/\partial U$ and the value that $\bar{\mu}$ takes at this point.

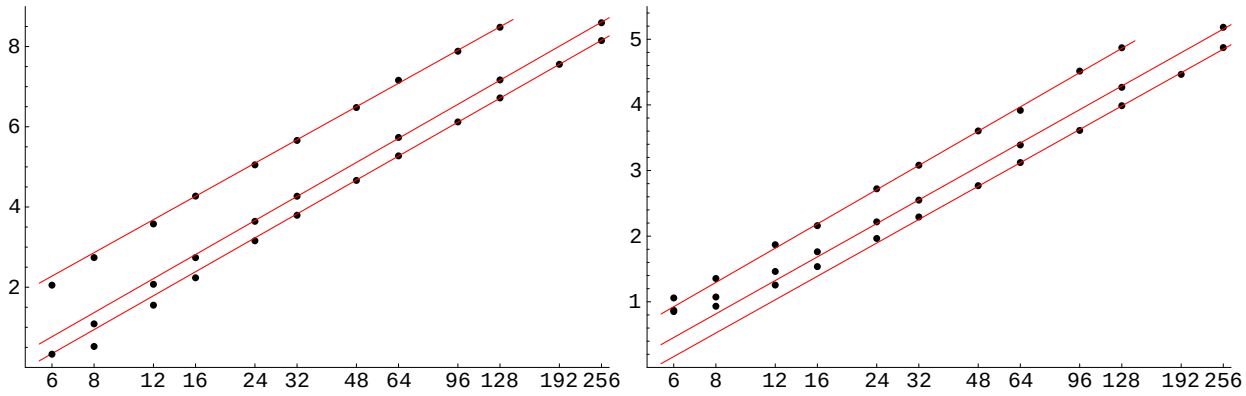

FIG. 24: Left: $\log\max\bar{\chi}(U)$ vs $\log L$ for the diamond, fcc and bcc lattice (downwards). Right: $\log\max\partial Q/\partial U$ vs $\log L$ for the diamond, fcc and bcc lattice (downwards).

which unfortunately does not intersect since the result for the diamond lattice disagree somewhat with the others. Still, the deviation is comparatively small.

The same holds for the maximum derivative of the magnetisation with respect to the

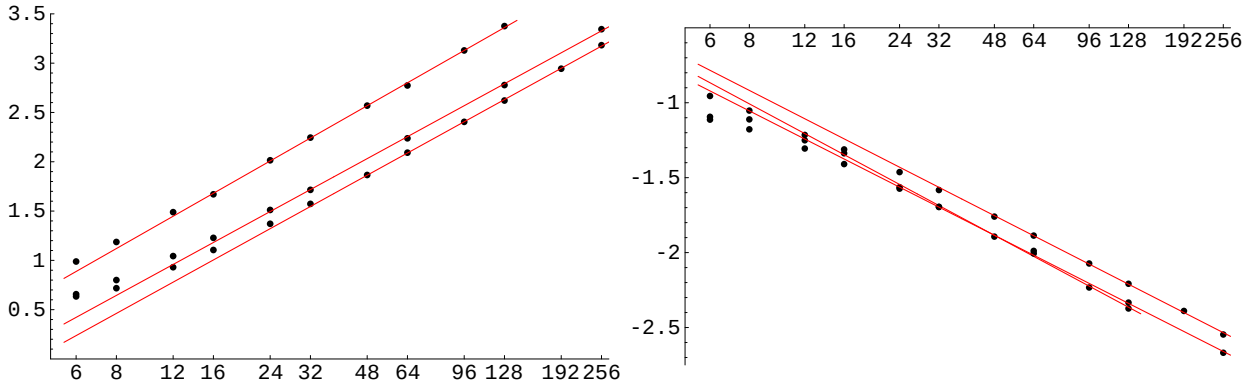

FIG. 25: Left: $\log \max \partial\bar{\mu}/\partial U$ vs $\log L$ for the diamond, fcc and bcc lattice (downwards). Right: $\log \bar{\mu}$ at the maximum derivative vs $\log L$ for the bcc, fcc and diamond (barely distinguishable) lattice (downwards).

energy, see left plot of Figure 25. The growth rate is

$$\begin{aligned} \text{sc} \quad & \lambda = 0.80 \pm 0.025 \\ \text{bcc} \quad & \lambda = 0.77 \pm 0.01 \\ \text{fcc} \quad & \lambda = 0.78 \pm 0.02 \\ \text{d} \quad & \lambda = 0.82 \pm 0.02 \end{aligned} \tag{17}$$

which do not intersect, though they all intersect with the interval for the sc lattice. The right plot of Figure 25 shows the magnetisation at this point where the maximum derivative occurs. The slopes ended up as

$$\begin{aligned} \text{sc} \quad & \lambda = -0.47 \pm 0.01 \\ \text{bcc} \quad & \lambda = -0.46 \pm 0.01 \\ \text{fcc} \quad & \lambda = -0.47 \pm 0.01 \\ \text{d} \quad & \lambda = -0.48 \pm 0.01 \end{aligned} \tag{18}$$

which all intersects in the common point $\lambda = -0.47$.

C. Critical exponents

There are of course combinatorial counterparts to the exponents in Section III D. As we have mentioned earlier, the fact that the specific heat grows to infinity corresponds to $\partial K/\partial U$ going to zero. Thus, α and α' correponds to the exponents a and a' respectively,

defined as

$$\begin{aligned} a &= \lim_{U\to U_c^-} \lim_{L\to\infty} \frac{\log K_L'(U)}{\log|U-U_c|} \\ a' &= \lim_{U\to U_c^+} \lim_{L\to\infty} \frac{\log K_L'(U)}{\log|U-U_c|} \end{aligned} \tag{19}$$

The exponents can be translated directly through some elementary algebra as

$$a = \frac{\alpha}{1-\alpha}, \qquad a' = \frac{\alpha'}{1-\alpha'} \tag{20}$$

Analogously for the exponents γ and γ' there is a microcanonical version of these as well

$$\begin{aligned} g &= \lim_{U\to U_c^-} \lim_{L\to\infty} \frac{-\log\bar{\chi}_L(U)}{\log|U-U_c|} \\ g' &= \lim_{U\to U_c^+} \lim_{L\to\infty} \frac{-\log\bar{\chi}_L(U)}{\log|U-U_c|} \end{aligned} \tag{21}$$

and for these we have

$$g = \frac{\gamma}{1-\alpha}, \qquad g' = \frac{\gamma'}{1-\alpha'} \tag{22}$$

For the magnetisation we then have the exponent b defined as

$$b = \lim_{U\to U_c^+} \lim_{L\to\infty} \frac{\log\bar{\mu}_L(U)}{\log|U-U_c|} \tag{23}$$

and it relates to β as

$$b = \frac{\beta}{1-\alpha'} \tag{24}$$

It is not neccesarily easier to study the microcanonical exponents rather than their canonical counterparts though. Especially exponent a seems difficult to estimate. In Figure 26 we plot the quotient part of the definition of a and a'. Since we do not wish to go too close to U_c we have stopped at the points where $\partial^2 K/\partial U^2$ has a minimum ($U \to U_c^-$) or a maximum ($U \to U_c^+$). We would hope for them to have roughly the same slope but the diamond lattice seems to prefer it otherwise. Since none of the curves show any sign of having achived a linear behaviour yet we will refrain from guessing at a. However, the right part of the figure, where the slope of the curves estimate a', seems better suited to the notion of them being equal. The estimates for the sc lattice were considerably lower, around 0.26 but were also based on larger lattices, which means that we may go even closer to U_c. Strangely, the

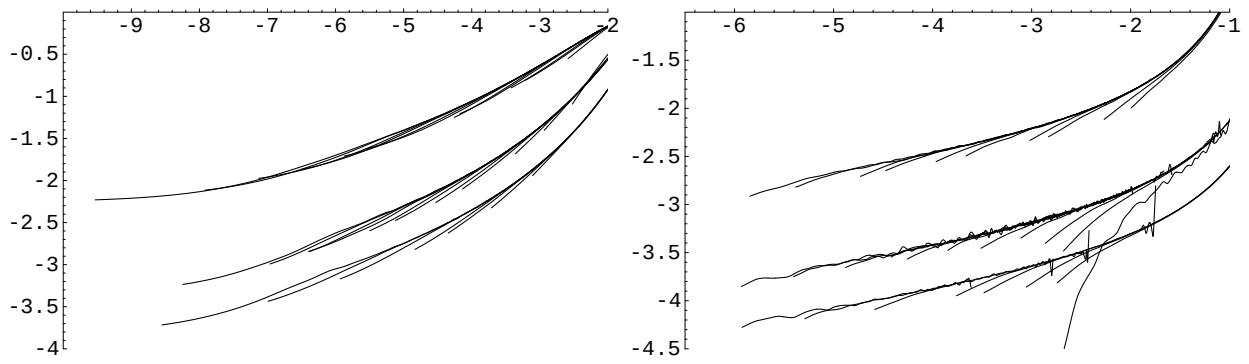

FIG. 26: $\log \partial K/\partial U$ vs $\log |U - U_c|$ for $U < U_c$ (left) and $U > U_c$ (right) for the diamond, bcc and fcc lattice (downwards) and all linear orders.

situation is somewhat better for a'. Here we obtained

$$\begin{aligned} \text{sc} \quad & a' = 0.195 \pm 0.015 \\ \text{bcc} \quad & a' = 0.21 \pm 0.02 \\ \text{fcc} \quad & a' = 0.215 \pm 0.01 \\ \text{d} \quad & a' = 0.22 \pm 0.01 \end{aligned} \tag{25}$$

which agree on the point $a' = 0.21$

For exponents g and g' we turn to Figure 27. The curves for the three lattices become very hard to distinguish, suggesting a small difference of the exponents. A more detailed scrutiny gives

$$\begin{aligned} \text{sc} \quad & g = 1.55 \pm 0.05 \\ \text{bcc} \quad & g = 1.60 \pm 0.15 \\ \text{fcc} \quad & g = 1.58 \pm 0.07 \end{aligned} \tag{26}$$

where we leave out the diamond, since no clear linear behaviour is seen yet (this is hidden in the muddle of the figure though). These three agree on the interval $g = 1.55 \pm 0.05$. For g' we received the estimates

$$\begin{aligned} \text{sc} \quad & g' = 1.50 \pm 0.05 \\ \text{bcc} \quad & g' = 1.45 \pm 0.10 \\ \text{fcc} \quad & g' = 1.50 \pm 0.10 \\ \text{d} \quad & g' = 1.68 \pm 0.08 \end{aligned} \tag{27}$$

which do not intersect due to the diamond lattice (which has only begun to show a linear behaviour). The other lattices intersect on the interval $g' = 1.50 \pm 0.05$ though.

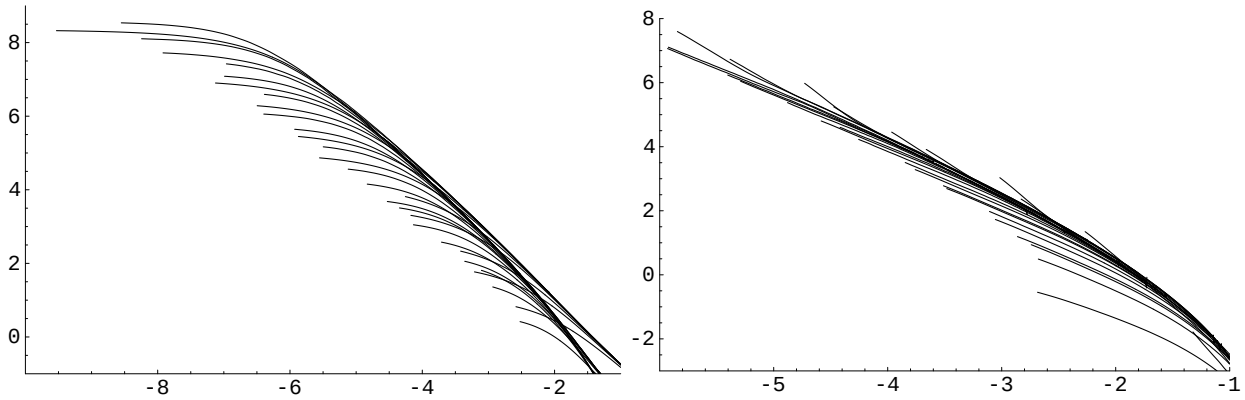

FIG. 27: $\log \bar{\chi}$ vs $\log |U - U_c|$ for $U < U_c$ (left) and $U > U_c$ (right) for the diamond, bcc and fcc lattice and all linear orders.

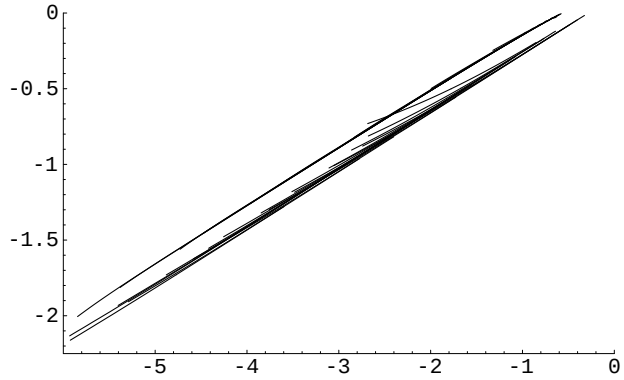

FIG. 28: $\log \bar{\mu}$ vs $\log |U - U_c|$ for $U > U_c$ for the diamond, bcc and fcc lattice (downwards) and all linear orders.

Our last exponent is b, see Figure 28, which shows a remarkably crisp behaviour for all lattices. They seem to have very similar slopes and indeed we obtained

$$\begin{aligned} \text{sc} \quad & b = 0.376 \pm 0.004 \\ \text{bcc} \quad & b = 0.380 \pm 0.005 \\ \text{fcc} \quad & b = 0.382 \pm 0.003 \\ \text{d} \quad & b = 0.387 \pm 0.007 \end{aligned} \tag{28}$$

which agree on the common point $b = 0.380$.

V. DISCUSSION

We have followed the method described in [14] and [15], just as in [13], to obtain sampled data of the bcc, fcc and d lattice for comparison with the sc lattice. The data gave us

	K_c	$\mathcal{U}_c$	$\mathcal{F}_c$	$\mathcal{S}_c$
sc	0.2216546(3)	0.33021(1)	0.7778503(2)	0.55827(1)
bcc	0.157371(1)	0.27261(4)	0.754006(1)	0.58240(3)
fcc	0.102069(1)	0.24676(6)	0.741740(2)	0.59062(4)
d	0.369722(7)	0.43161(9)	0.833356(6)	0.51421(7)

TABLE XIX: Critical parameters for the different lattices. The values for sc are taken from [13].

estimates of the critical temperatures and other parameters, see Table XIX. Especially for fcc and bcc they are of good quality, but somewhat less so for the d lattice. We have also tried to estimate the high- and low-temperature exponents separately, both the canonical ones (α, α', etc) and the microcanonical ones (a, a', etc), as well as the growth rate at local maxima/minima of various quantities, eg the maximum specific heat and susceptibility.

The 3-dimensional lattices indeed show a similar behaviour near the critical temperature. What seems to be the characteristic behaviour here is that the exponents between the lattices are similar but also show different high- and low-temperature exponents, see Table XX. Though the data suggest that α', β, γ, γ' and δ have the same value for different lattices, at least up to the precision we can aspire to, there are also glaring problems with some estimates, such as α. Here the value for sc is smaller than for the other lattices. With some certainty this can be explained by the fact that the bcc, fcc and d lattices used here are smaller than those used for the sc lattice, especially so for the d lattice. The exponents can only be established with some accuracy when a clearly linear behaviour is shown in the log-log plots and this is not the case for our lattices when it comes to α. Accurate estimates may very well require quite large lattices, but the data lends no support to the claim that α and α' are equal. Exponents γ and γ' are rather well-behaved though and the data consistently tend to give us different values for each lattice, though fairly equal between lattices. However, taking into account the sometimes rather wide error estimates we can no longer be certain, since the intervals for γ and γ' intersects for bcc and fcc, but the sc and d lattice prefers to keep them apart. We have listed other estimates in Table XX obtained through different methods. The values from [5] are obtained through merged Monte Carlo results for ν and η from spin-1 Ising model and the ϕ^4 theory. The listed exponents are then obtained using the standard scaling relations. The exponents from [6] were obtained through

	α	α'	β	γ	γ'	δ
ϕ^4 [5]	0.1109(15)		0.3262(4)	1.2366(15)		4.791(9)
FT [6]	0.1091(24)		0.3257(5)	1.2403(8)		4.808(8)
HT [11]	0.1094(12)		0.3265(7)	1.2375(6)		4.79(1)
HT [10]	0.1096(5)		0.32653(10)	1.2373(2)		4.7893(8)
MCRG [8]	0.1073(36)		0.3274(9)	1.2378(27)		4.78(2)
LT [9]		0.112(11)	0.324(2)		1.24(1)	4.83(5)
sc	0.220(15)	0.164(7)	0.323(8)	1.205(25)	1.265(15)	4.88(3)
bcc	0.275(25)	0.177(12)	0.325(8)	1.230(15)	1.285(40)	4.9(1)
fcc	0.27(2)	0.17(2)	0.325(2)	1.24(2)	1.26(2)	5.0(1)
d	0.26(2)	0.187(13)	0.33(1)	1.225(25)	1.32(6)	5.1(1)

TABLE XX: Critical exponents for the different lattices. The values for sc are taken from [13].

field-theoretic methods and the standard scaling relations. For [11] and [10] the values were found through high-temperature series expansions of the bcc and sc lattice respectively. In [8] the Monte Carlo renormalization group was used. Finally, for [9] the authors used low-temperature series expansion. In references [5, 6, 8–11] it was assumed that the scaling hypothesis holds so that high- and low-temperature exponents are equal. Consequently, none of these references measure α and α' explicitly.

As we have seen throughout the paper the least-assumptions fit to our sampled data is most easily reconciled with a picture where high- and low-temperature exponents differ, but where any given exponent could very well have one and the same value for all the different lattices under consideration. If this picture is correct we have a scenario for the critical regime which is at the same time very familiar (ie the exponents agree between the lattices) and very different (ie different high- and low-temperature exponents) from the working assumption of statistical physics during the last 30 years. In the 1960's scaling relations were considered beautiful hypotheses, but with no motivating mechanism many considered them almost too good to be true [23]. This all changed with the arrival of Wilson's renormalisation theory [4]. Suddenly there was a widely applicable theory which provided an explanation for many scaling hypotheses and also made it plausible that there were in fact only a smaller number of distinct types of critical behaviour, the so called universality classes. See [24] for

an extensive survey. Motivated by this the scaling relations soon became important tools in the analysis of Monte Carlo data, even though some voiced important concerns about the practices of many standard simulations [21], and when adressing those concerns also began to see deviations from the mainstream results.

Now, the scaling relations are both one of the principal predictions of standard renormalisations theory and in direct conflict with the existence of models where the high- and low-temperature exponents differ, ie exactly the scenario we may have found. On the other hand, the existence of universality classes has also to a large extent been motivated by renormalisation theory, and the existence of a common behaviour for the Ising model on the 3-dimensional lattices is also in agreement with our data. So we are faced with a situation where we either have to believe that finite-size corrections far beyond those usually assumed mask the asymptotic behaviour of the Ising even on the largest lattices used today [13], or standard renormalisation theory fails, due to the conflict between its scaling predictions and distinct low- and high-temperature behaviours. In the latter, and probably in the eyes of many, more extreme case, one would then suddenly need to find either a non-differentiable version of the renormalisation theory, which is consistent with the many caveats from [25], or an entirely new mechanism explaining the persistence of the universality class concept. Here all the options presented seem to offer bountiful opportunities for further investigation.

Acknowledgements

This research was conducted using the resources of High Performance Computing Center North (HPC2N) and the Center for Parallel Computers (PDC). The research was financed by the Swedish Research Council (VR) which we would like to thank. One of the authors (AR) would like to thank James L Smith for his continuous support over the years.

---

[1] E. Ising, Z. Physik **31**, 253 (1925).

[2] L. Onsager, Phys. Rev. (2) **65**, 117 (1944).

[3] L. P. Kadanoff, Physics **2**, 263 (1966).

[4] K. G. Wilson, Phys. Rev. D (3) **2**, 1438 (1970).

[5] M. Hasenbusch, Int. J. Mod. Phys. C **12**, 911 (2001).

[6] F. Jasch and H. Kleinert, J. Math. Phys. **42**, 52 (2001).

[7] R. Gupta and P. Tamayo, Int. J. Mod. Phys. C **7**, 305 (1996).

[8] H. W. J. Blöte, J. R. Heringa, A. Hoogland, E. W. Meyer, and T. S. Smit, Phys. Rev. Lett. **76**, 2613 (1996).

[9] Z. Salman and J. Adler, Int. J. Mod. Phys. C **9**, 195 (1998).

[10] M. Campostrini, A. Pelissetto, P. Rossi, and E. Vicari, Phys. Rev. E **65**, 066127 (2002).

[11] P. Butera and M. Comi, Phys. Rev. B **62**, 14837 (2000).

[12] A. Pelissetto and E. Vicari, Phys. Rep. **368**, 549 (2002), ISSN 0370-1573.

[13] R. Häggkvist, A. Rosengren, P. H. Lundow, K. Markström, D. Andrén, and P. Kundrotas, Adv. Phys. **56**, 653 (2007).

[14] R. Häggkvist, A. Rosengren, D. Andrén, P. Kundrotas, P. H. Lundow, and K. Markström, J. Statist. Phys. **114**, 455 (2004).

[15] P. H. Lundow and K. Markström, arXiv:cond-mat/0612465.

[16] M. E. J. Newman and G. T. Barkema, *Monte Carlo methods in statistical physics* (The Clarendon Press Oxford University Press, New York, 1999), ISBN 0-19-851796-3; 0-19-851797-1.

[17] Y. Murase and N. Ito, J. Phys. Soc. Jpn. **77**, 014002 (2008).

[18] C. Domb, in *Phase transitions and critical phenomena, Vol. 3*, edited by C. Domb and M. S. Green (Academic Press, London, 1974), pp. 357–484.

[19] Y. Deng and H. W. J. Blöte, Phys. Rev. E **68**, 036125 (2003).

[20] O. G. Mouritsen, J. Phys. C: Solid St. Phys. **13**, 3909 (1980).

[21] G. A. Baker, Jr. and N. Kawashima, J. Phys. A **29**, 7183 (1996), ISSN 0305-4470.

[22] D. Andrén, arXiv:0706.3116v1.

[23] M. Fisher, in *Lecture notes in theoretical physics, Vol. VII.c* (University of Colorado Press, Boulder, 1964), pp. 1–159.

[24] J. Cardy, *Scaling and renormalization in statistical physics*, vol. 5 of *Cambridge Lecture Notes in Physics* (Cambridge University Press, Cambridge, 1996).

[25] A. C. D. van Enter, R. Fernández, and A. D. Sokal, J. Statist. Phys. **72**, 879 (1993).